Coulomb excitation study of ^{235}U: Assessment of theoretical quasiparticle states

J. de Bettencourt, Ch. Briançon, J. Libert, J. P. Thibaud, and R. J. Walen
Centre de Spectrométrie Nucléaire et de Spectrométrie de Masse, Orsay, France

A. Gizon
Institut des Sciences Nucléaires, Grenoble, France

M. Meyer
Institut de Physique Nucléaire, Lyon, France

Ph. Quentin
Laboratoire de Physique Théorique, Université de Bordeaux I, Gradignan, France
(Received 5 February 1986)

Coulomb excitation experiments have been performed on ^{235}U targets with 370 and 450 MeV ^{84}Kr projectiles. The deduced experimental level scheme exhibits 11 band structures developed up to high spins. A rotor-plus-quasiparticle microscopic approach, free of any *ad hoc* parameter adjustment, has been applied to this nucleus yielding a very good reproduction of band-head energies, moments of inertia, multipole moments, and transition probabilities, which assesses the relevance of the underlying Hartree-Fock plus BCS mean field description.

I. INTRODUCTION

Coulomb excitation induced by heavy ions is a very powerful tool for studying collective band structures related to the ground state of a given nucleus. Recently, such experiments using very heavy projectiles such as ^{84}Kr, ^{208}Pb, ^{232}Th, and ^{238}U have been performed in even-even actinide isotopes (for a reference list see, for example, Refs. 1–3). These experiments show that high spin states of the ground band are especially well excited but, in addition, they reveal very nicely collective vibrational spectra as quadrupole and octupole degrees of freedom.

A detailed understanding of rotational spectra at high angular momentum has been established in rare-earth isotopes where the $i\frac{13}{2}$ neutron excitations are responsible for strong irregularities in the spectra due to the large Coriolis forces associated with high-j particles. Similar conditions do exist in the actinides where both $i\frac{13}{2}$ proton and $j\frac{15}{2}$ neutron orbitals lie close to the Fermi surface.

In odd-A nuclei, Coulomb excitation is, in addition, an efficient tool for exciting rotational bands based on quasiparticle states coupled by Coriolis mixing to the ground-state configuration.

The ^{235}U nucleus indeed appeared as a particularly good candidate to study in detail the nuclear structure at high spin, with its ground state $\frac{7}{2}^-[743]$, belonging to the $j\frac{15}{2}$ subshell, well separated in energy from the other negative-parity subshells. This feature has suggested the present study of ^{235}U by Coulomb excitation using krypton ions and performing high-statistics γ-γ coincidence measurements.

From the previous experiments performed in ^{235}U using Coulomb excitation with lighter projectiles such as ^{4}He, ^{16}O, and ^{40}Ar, it appeared, as expected, that the $\frac{7}{2}^-[743]$ ground band was predominantly excited.[4] In addition, a few members of other rotational bands were observed with significant intensities. Therefore it appeared that Coulomb excitation induced by projectiles heavier than ^{40}Ar could deliver much new information on ^{235}U. The recent experiments with ^{208}Pb projectiles indeed yield informations up to very high spin ($\frac{55}{2}^-$) in the ground band.[5,6]

The aim of the present work is the detailed experimental study of the rotational sidebands and the theoretical description of their properties within a rotor plus quasiparticle approach.

In Sec. II the experimental procedure is briefly described and the bulk of the results is given. We discuss the data and present the deduced level scheme in Sec. III, while in Sec. IV the theoretical interpretation of the whole scheme is proposed within the framework of a rotor plus quasiparticle approach using Hartree-Fock plus BCS single-particle states.

II. EXPERIMENTAL PROCEDURES AND RESULTS

In the present experiment, multiple Coulomb excitation of ^{235}U has been studied by means of high-resolution gamma-ray spectroscopy. A 0.1 mm metallic foil with 80% isotopic enrichment in mass 235, 10% in mass 234, and 10% in mass 238 has been bombarded with the ^{84}Kr beam of the ALICE cyclotron of the Institut de Physique Nucleaire at Orsay. Two bombarding energies were used: 370 MeV, i.e., well below the Coulomb barrier, and 450 MeV, closer to the barrier but still with negligible contribution from reaction and fission production.

The measuring setup shown in Fig. 1 consisted of two large Ge-Li detectors located on both sides of the target, at 3 cm distance, and at 90° with respect to the beam axis.

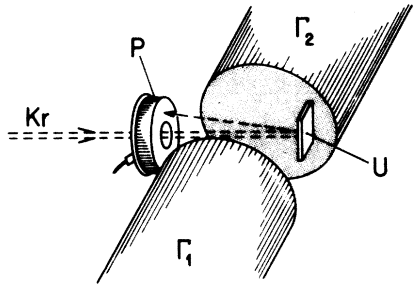

FIG. 1. Experimental setup to study Coulomb excitation of ^{235}U with ^{84}Kr projectiles. The annular particle detector was protected against x rays and electrons by a thin gold foil. It detected scattered krypton projectiles in an angle of 133°–147° with respect to the beam axis. The two γ counters, γ_1 and γ_2, were located at 90° on either side of the incident beam.

A 40 mm diam annular detector (a boron implanted silicon diode) detected the krypton ions scattered between 133° and 147° with respect to the beam. The data measured were the two direct γ spectra (γ_1 and γ_2), the scattered particle spectrum, the particle-γ and γ_1-γ_2 coincidences, and the corresponding time spectra.

In the singles spectra, the ratio of the intensities of the γ lines for the two bombarding energies was used to make a crude classification of the spin heights of the levels into low, medium, and high values.

With krypton projectiles, the stopping time of the recoiling nucleus in the material of the target is of the order of the lifetime of the highest excited states. In the actinides, typical values of the lifetimes of the yrast states with spin $\sim 20\hbar$ are of the order of the picosecond, so that the Doppler effect is negligible, except for the last excited states. Nevertheless, the geometry of the two Ge-Li detectors positioned at $\pm 90°$ to the beam axis allows observation of those γ transitions where the emitting nucleus is still in flight. The line observed is then broadened but not notably Doppler shifted. The backward geometry of the particle detector was chosen so as to favor, in particle-γ coincidence measurements, the detection of the γ transitions associated with the highest spin states.

Figure 2 shows a singles spectrum, while Fig. 3 shows a γ spectrum gated by the backscattered particles. The comparison of these spectra exhibits clearly the interest of particle-gamma coincidences which lower considerably the background and strengthen the γ rays of the ground band which cascade from the highest spin states populated in the multiple Coulomb excitation.

High-statistics γ-γ coincidence measurements have been performed at 450 MeV incident energy. The data recorded sequentially event by event on magnetic tapes were analyzed off line with a program allowing a representation in 2^{24} channel two-dimensional matrices. To illustrate these measurements, a total projection of the γ-γ coincidence spectra is shown in Fig. 4.

The summary of the information on energies, intensities, and assignments is given in Table I. In this study about 400 transitions could be assigned, most of them observed in the coincidence spectra.

III. THE LEVEL SCHEME

The level scheme proposed in the present work has been established on the basis of the results presented in Table I, also using energy sum rules and the analysis of feeding and deexcitation properties of the states. The informations on the well-established low-spin part of some of the bands have been used.[7] The experiments including multipolarity measurements[4,8] provide especially important grounds for the analysis.

In this section we present the various bands observed. Besides the ground-state band, the other negative-parity and positive-parity bands are successively given. In order to show how the bands are related, a diagram is given for each of them, presenting the feeding and the deexcitation of each state. In a way, this procedure gives a kind of model-independent level scheme, exhibits the main connections between the bands, and emphasizes the configuration mixings and the presence of vibrational modes. At the end of this section, a summary of the observed rotational bands is given. To make the following description of the states as clear as possible, we shall label the bands by the usual Nilsson quantum numbers of the main component of the states, as will be justified in Sec. IV.

A. The negative parity bands

Besides the ground state $\frac{7}{2}^-[743]$ band, mainly excited in this Coulomb excitation experiment, other negative parity bands were also identified and associated with either quasiparticle configurations issued from the $j\frac{15}{2}$ subshell, or vibrational modes built on the ground configuration.

1. The ground-state $\frac{7}{2}^-$ | 743 | band

The ground-state rotational band, based on the $\frac{7}{2}^-[743]$ state, is predominantly excited in our experiments. In the most complete measurements prior to this work, states up to spin $I^\pi = \frac{25}{2}^-$ at 805 keV have been observed.[4] In our measurements,[9,10] states up to spin $I^\pi = \frac{47}{2}^-$ at 2830 keV have been Coulomb excited and their assignment results from the γ-γ coincidences. The $I+1 \rightarrow I$ transitions are observed up to the $\frac{31}{2}^-$ state (see Fig. 5). The energy level spacing appears to be rather regular, and characteristics such as the moment of inertia and the Coriolis coupling effects will be discussed in the next section.

This set of precise results has been used as a basis in the analysis of the more recent measurements of high-spin states in the ^{235}U ground band, undertaken at the Gesellschaft für Schweren Ionen UNILAC accelerator at Darmstadt, with ^{208}Pb ions.[5,6] As also observed in these experiments, we notice a pronounced intensity jump (see Fig. 3) between the $\frac{23}{2}^- \rightarrow \frac{19}{2}^-$ and the $\frac{21}{2}^- \rightarrow \frac{17}{2}^-$ γ transitions. This is due to a change in the branching ratios between the $\Delta I = 2$ and 1 transitions above the $\frac{21}{2}^-$ level: the energy of the $M1$ ($\Delta I = 1$) transitions exceeds then the K conversion threshold, so that an increasing intensity is going through these highly converted $M1$ transitions, diminishing the branching ratio of $\Delta I = 2$ against $\Delta I = 1$ transitions.

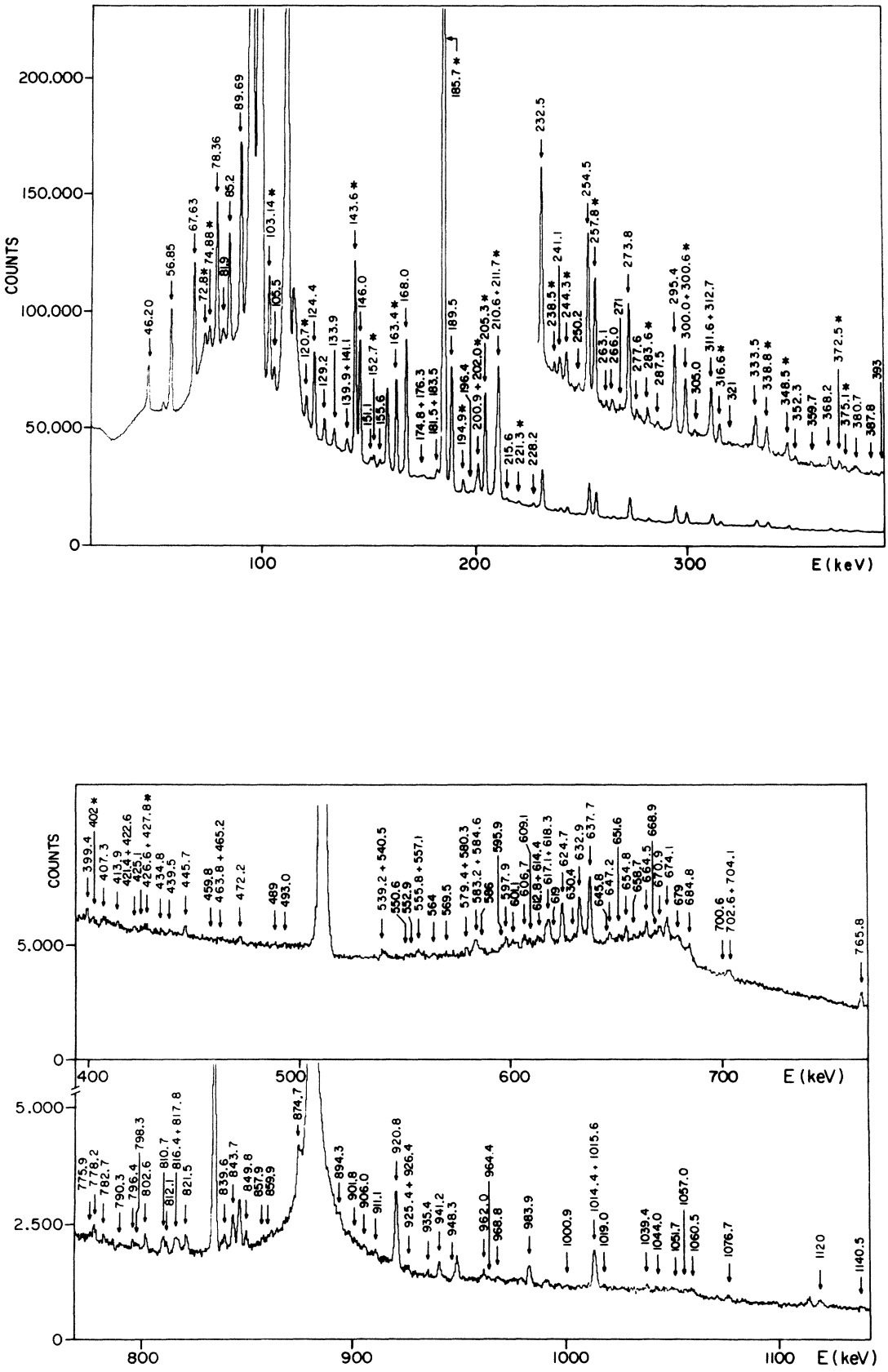

FIG. 2. Singles γ spectra observed in Coulomb excitation of ^{235}U with krypton beam at 470 MeV. In case of complex lines, the indicated energy is the one of the main component. The lines marked by a star are attributed to impurities (^{234}U, ^{238}U, and radioactivity).

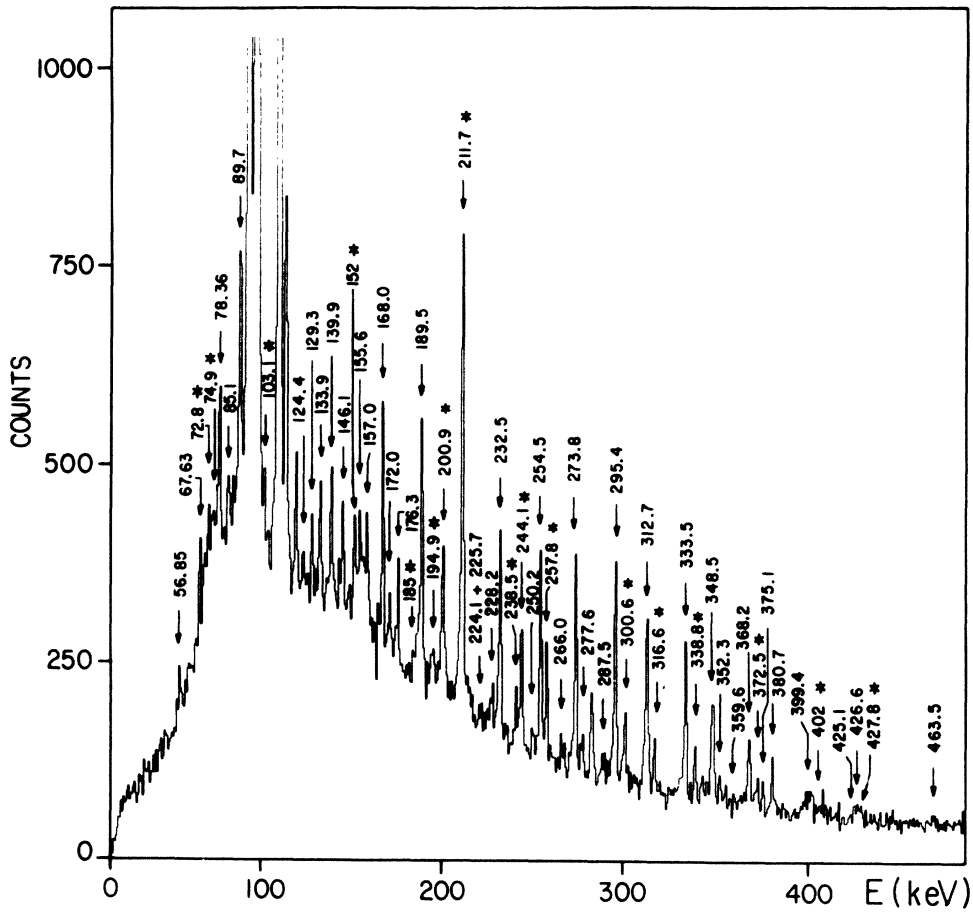

FIG. 3. Gamma spectrum observed in coincidence with the scattered particles. The reaction conditions are the same as in Fig. 2.

2. *The* $\frac{5}{2}^-[752]$ *band*

This rotational band, based on the 632.9 keV level, has been observed in Ref. 4 up to the $\frac{13}{2}^-$ state. The value $K=\frac{5}{2}$ has been assigned according to the deexcitation properties (dominant $M1$ type transitions) of the states to the ground band. This K value is also supported by (n,γ), transfer, and (d,d') reaction measurements.[8,11,12]

In the present experiment the sequence of the lowest states is in good agreement with the previous proposed scheme. Similarly, we have observed that these states deexcite mainly to the ground band. Moreover, our γ-γ coincidence data show several groups of transitions connecting this band to other ones, allowing us to extend knowledge of this band up to the $\frac{25}{2}^-$ state. Indeed, as shown in Fig. 6, each level of this band also decays to the states of the $\frac{1}{2}^+[631]$, $\frac{7}{2}^+[624]$, and $\frac{3}{2}^+[631]$ bands. Furthermore, the band is populated by deexcitations of states of other bands lying higher in energy, i.e., $\frac{9}{2}^-[734]$, $\frac{3}{2}^-[761]$, $\frac{3}{2}^-\{\frac{7}{2}^-[743],2_\gamma^+\}$, and $\frac{11}{2}^-\{\frac{7}{2}^-[743],2_\gamma^+\}$ bands, all related to the $j\frac{15}{2}$ shell. We observe also intraband $\Delta I=1$ and 2 transitions. The spin assignments of the successive states of this $\frac{5}{2}^-[752]$ band have been determined from the lowest state, $\frac{5}{2}^-$, at 632.9 keV up to the highest observed state, $\frac{25}{2}^-$, at 1490 keV, using all these sets of intraband and interband transitions in a self-consistent way.

The level spacing in this band appears to be less regular as compared to the ground-state band.

3. *The* $\frac{9}{2}^-[734]$ *band*

A $K=\frac{9}{2}$ rotational band, based on a state at 822 keV with two excited levels at 886 and 961 keV, was previously proposed[4] according to the $M1$ multipolarity of the transitions decaying to the ground band. This assignment was also confirmed through (d,d') experiments.[12,13]

In the present measurements, this band has been identified again and extended up to the $\frac{23}{2}^-$ state. This set of levels has been obtained essentially through the γ-γ coincidence data. The two intraband cascades, 138.4, 190.8, 241.1 keV and 159.7, 205.4, 244.3 keV, have been identified. The band has a strong decay to the ground and the $\frac{5}{2}^-[752]$ bands and a weaker deexcitation to the $\frac{11}{2}^-\{\frac{7}{2}^-[743],2_\gamma^+\}$, $\frac{7}{2}^+[624]$, and $\frac{1}{2}^+[631]$ bands. A strong population of the states arises from the $\frac{3}{2}^-[761]$ band and a weaker one from the $\frac{11}{2}^-\{\frac{7}{2}^-[743],2_\gamma^+\}$ band. The partial level scheme related to the $K^\pi=\frac{9}{2}^-$ band is shown in Fig. 7. This band clearly has its strong-

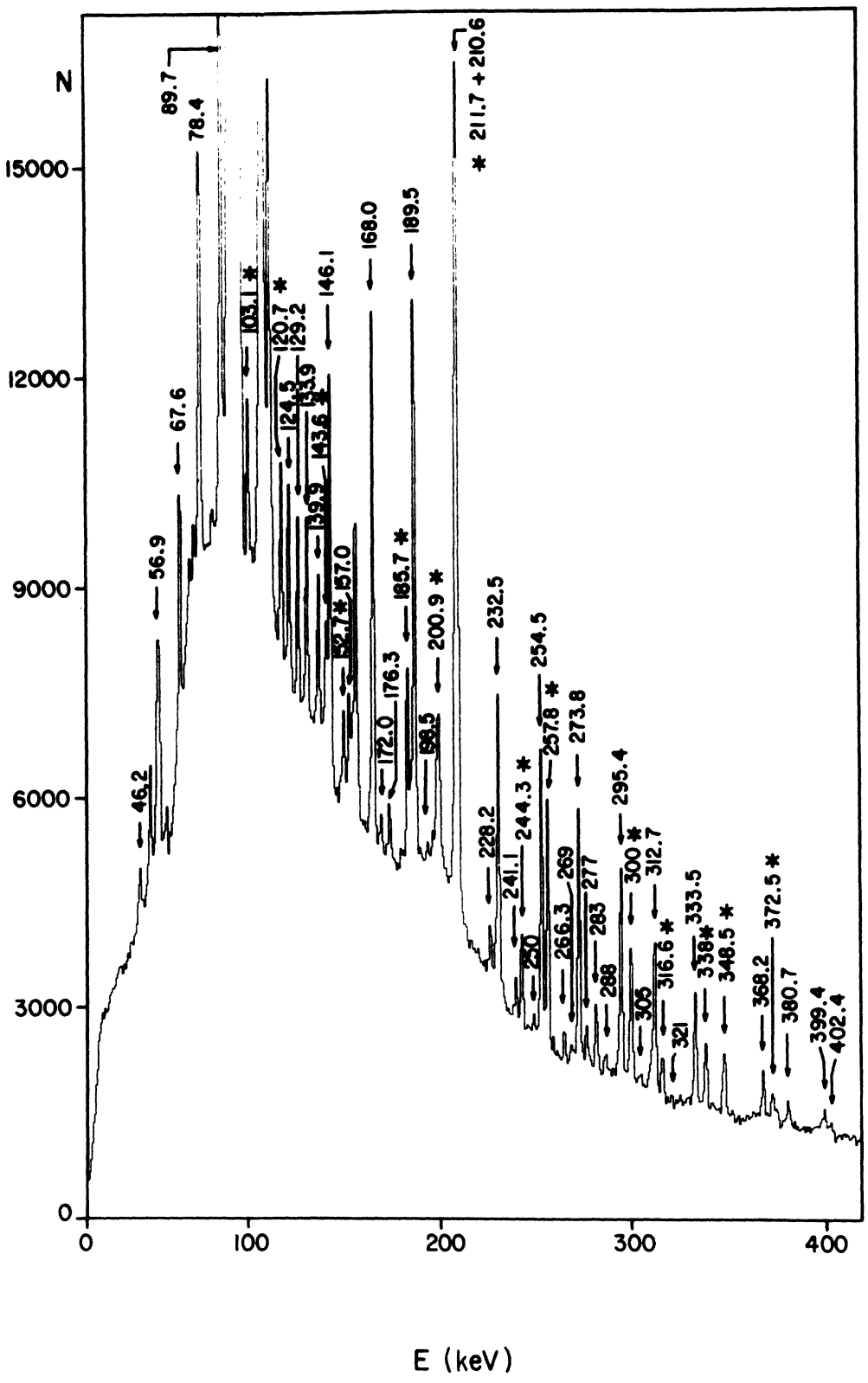

FIG. 4. Total projection of the coincidence γ-γ spectra.

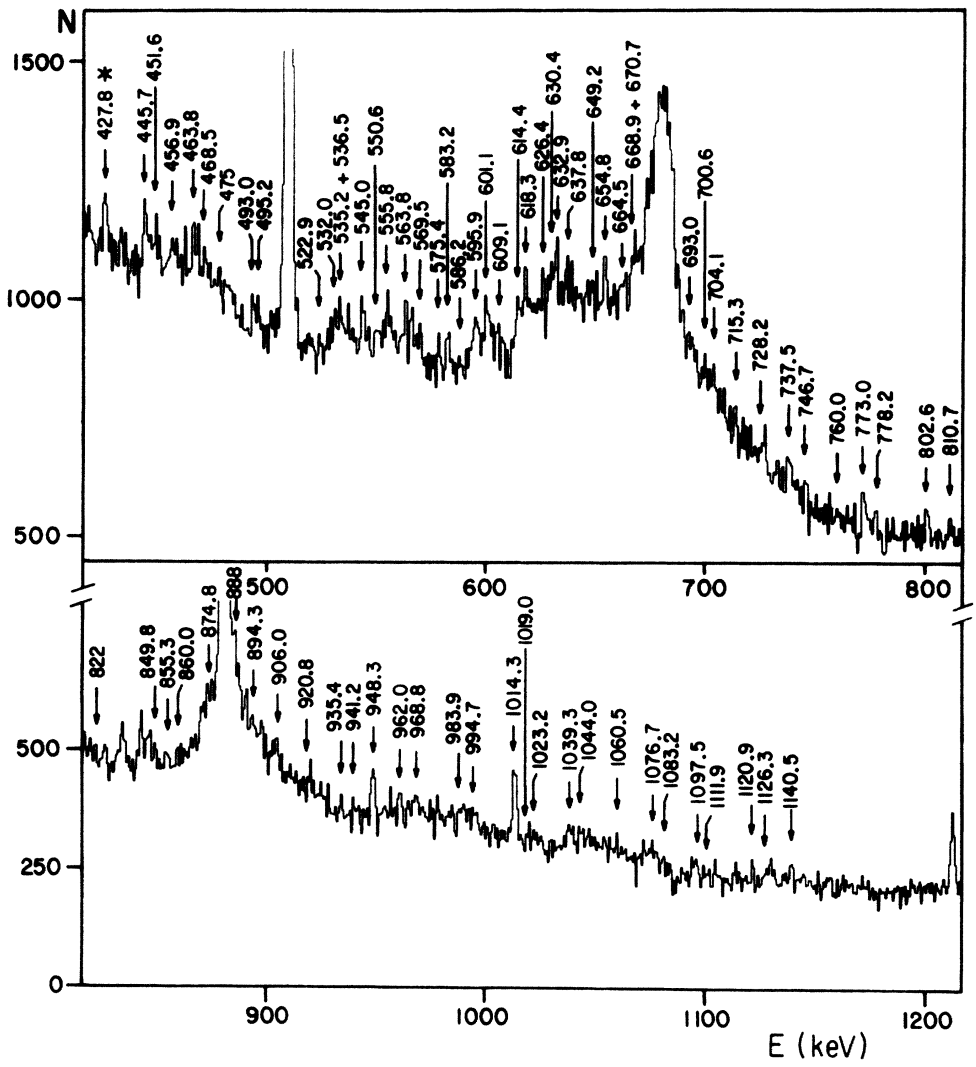

FIG. 4. (*Continued*).

est connections with bands which are based on $j^{\frac{15}{2}}$ orbital components.

4. The $\frac{3}{2}^-\{[761]+[741]\}$ band

Three levels—at 1039, 1061, and 1098 keV—were observed in previous experiments without precise assignment.[12–14] In our Coulomb excitation experiment, these levels have been found to be the three first members of a rotational band which is developed up to the $\frac{23}{2}^-$ state at 1647 keV, on the basis of its deexcitation paths toward eight bands (see Fig. 8). The strongest decay goes to the bands related to the $j^{\frac{15}{2}}$ orbitals: $\frac{7}{2}^-[743]$, $\frac{5}{2}^-[752]$, $\frac{9}{2}^-[734]$, $\frac{3}{2}^-\{\frac{7}{2}^-[743], 2_\gamma^+\}$. However, no decay has been observed to the $\frac{11}{2}^-\{\frac{7}{2}^-[743], 2_\gamma^+\}$ band. One also observes deexcitations to the low K positive-parity bands ($\frac{1}{2}^+[631]$, $\frac{3}{2}^+[631]$, $\frac{5}{2}^+[622]$, and $\frac{5}{2}^+[633]$, but none was found to the $\frac{7}{2}^+[624]$ band. These decay properties allow us to propose $K^\pi=\frac{3}{2}^-$ for this band. Moreover, its strong population by Coulomb excitation, even with a band head as high in energy as 1039.3 keV, and its deexcitation properties to the states related to the $j^{\frac{15}{2}}$ orbital strongly suggest the $\frac{3}{2}^-[761]$ assignment for this band. However, as discussed in Sec. IV, this pure assignment is not supported by the predictions of the rotor plus quasiparticle calculations which predict a mixture of both $\frac{3}{2}^-[761]$ and $\frac{3}{2}^-[741]$ configurations.

One may remark that this band is strongly perturbed, much more than the $\frac{5}{2}^-[752]$ band. This fact supports also the proposed interpretation of this $\frac{3}{2}^-$ band, which is expected to be strongly coupled with both $\frac{1}{2}^-[770]$ and $\frac{1}{2}^-[750]$ bands, well known for their large negative decoupling parameter.

5. The $\frac{3}{2}^-\{\frac{7}{2}^-[743], 2_\gamma^+\}$ band

From their Coulomb excitation measurements, Stephens *et al.*[4] have proposed three levels, at 638, 665,

TABLE I. Transitions observed in ^{235}U. Energy, intensity, and assignment of the transitions are given in the three first columns. For complex γ lines the total intensity is given. In the last column, *A* stands for transitions observed previously, *C* for transitions observed in γ-γ coincidence spectra in the present work, and *L* for the lowest intensity components within a complex line. Natural target radioactivity and background are indicated by PR (partly radioactive) and MR (mostly radioactive).

Energy (keV)	Relative intensity	Assignment Initial level	Assignment Final level	Comments
38.0±0.5		670.9	632.9	*C*
46.20±0.07		46.2	0	*A*
49.4±0.5		720.3	670.9	*C*
56.85±0.10		103.1	46.2	*A,C*
		777.3	720.3	*C*
63.5±0.5		701.0	637.8	*C*
		885.8	821.8	*C*
65.4±0.5		1126.3	1060.6	*C*
67.63±0.07		170.7	103.1	*A,C*
68.1±0.5		701.0	632.9	*C*
72.8±0.1		850.2	777.3	*C*,PR
		923.3	850.2	*C*
74.88±0.07		960.5	885.8	*C*,PR
		608.0	533.2	*C*
78.36±0.07		249.1	170.7	*A,C*
79.5±0.5		750.4	670.9	*C*
80.5±0.5		474.1	393.5	*C*
		413.2	332.8	*C*
81.89±0.10		690.2	608.0	*C*
85.15±0.12		1045.5	960.5	*C*
85.7±0.5		1107.2	1021.7	*C*
		454.5	369.0	*C*
		750.4	664.5	*C*
		805.9	720.2	*C*
87.5±0.5		720.3	632.9	*C*
88.8±0.5		1214.7	1126.3	*C*
		1186.5	1097.7	*C*
89.7±0.1		338.8	249.1	*A,C*
90.1±0.5		1155.3	1065.2	*C*
102.0±0.5	23±5	471.3	369.0	*C*
		661.2	559.4	*C*
103.0±0.5 103.1±0.1	570±30	793.8	690.2	*C,L* $^{238}U(4^+ \rightarrow 2^+)$
		103.1	0	*A,C*,PR
		1495.0	1392.1	*C*
104.9±0.5		151.0	46.2	*C,L*
		559.4	454.5	*C*
	90±9	805.9	701.0	*C*
		881.5	777.3	*C*
105.5±0.1		1151.2	1045.5	*C*
106.5±0.5		777.3	670.9	*C*
		533.4	426.7	*C*
108.7±0.5		885.8	777.3	*C*
109.9±0.5		359.0	249.1	*C*
115.5±0.5		197.0	81.8	*C*
116.2±0.5		129.3	13.0	*C,A*
117.5±0.5		750.4	632.9	*C*

TABLE I. (*Continued*).

Energy (keV)	Relative intensity	Assignment Initial level	Assignment Final level	Comments
119.3±0.5	150±10	290.5	171.4	*C,A,L*
		171.4	51.7	*C,L*
		532.4	413.2	*C,L*
120.7±0.1		671.1	550.4	*A,C*,PR
		1307.0	1186.5	*C*
122.1±0.2	38±4	1045.5	923.3	*C*,PR
122.3±0.5		413.2	290.5	*C,L*
123.7±0.5	460±20	1373.3	1250.0	*C,L*
		294.6	170.7	*C,L*
124.4±0.1		170.7	46.2	*A,C*
		1045.5	920.8	*C*
125.2±0.5		171.4	46.2	*C,L*
127.9±0.5	130±10	1456.8	1329.4	*C,L*
		687.3	559.4	*C,L*
		1235.2	1107.2	*C,L*
		1149.5	1021.7	*C,L*
129.2±0.1		129.3	0	*C,A*
		1151.2	1021.7	*C*
		568.0	438.6	*C*
		1329.4	1200.6	*C*
129.8±0.5		850.2	720.3	*C,L*
131.3±0.5	10±5	881.5	750.4	*C*
		1456.8	1325.8	*C*
132.5±0.5	100±10	720.3	587.8	*C,L*
133.9±0.1		805.0	671.1	*A,C*
		1155.3	1021.7	*C*
		608.0	474.1	*C*
135.0±0.5		805.9	670.9	*C,L*
138.3±0.5	85±7	960.5	821.8	*C,L*
		1456.8	1318.5	*C,L*
139.9±0.1		944.9	805.0	*C*
		290.5	151.0	*C*
		1031.5	891.8	*C*
		1063.2	923.3	*C*
141.1±0.1	36±5	1392.1	1250.9	*C*
		1186.5	1045.5	*C*
142.4±0.5	940±50	750.4	608.0	*C,L*
		509.8	367.0	*C,L*
		587.8	445.7	*C,L*
		1250.0	1107.2	*C,L*
143.6±0.1		923.3	780.0	*C*,PR
		1250.9	1107.2	*C*
		920.8	777.3	*C*
		294.6	151.0	*C*
		225.4	81.8	*C,A*
		369.0	225.4	*C*
144.4±0.5	11±4	1065.2	920.8	*C*
		1473.5	1329.4	*C*
		616.4	471.3	*C*
146.0±0.5	670±40	1635.7	1490.2	*C,L*
146.1±0.1		249.1	103.1	*A,C*
		923.3	777.3	*C*
		485.0	338.8	*C,L*
147.5±0.5		953.4	805.9	*C*
150.2±0.5	5±3	682.7	532.4	*C*

TABLE I. (*Continued*).

Energy (keV)	Relative intensity	Assignment Initial level	Assignment Final level	Comments
151.1±0.1	44±3	821.8	670.9	*C*
151.7±0.5		1647.0	1495.0	*C,L*
152.7±0.1	64±4	1459.8	1307.2	*C*, mainly $^{234}U(6^+ \rightarrow 4^+)$
154.2±0.5	~3	825.2	671.1	*C*
155.0±0.5	52±5	687.3	532.4	*C,L*
155.5±0.1		1390.5	1235.2	*C*
		1100.4	944.9	*C*
157.0±0.1	33±4	1647.0	1490.2	*C*
		1257.5	1100.4	*C*
		1392.1	1235.2	*C*
		690.2	533.2	*C*
160.1±0.2	52±7	454.5	294.6	*C*
		1045.5	885.8	*C*
		953.4	793.8	*C*
161.2±0.3	12±3	332.8	171.4	*C,A*
		881.5	720.3	*C*
		670.9	509.8	*C*
161.9±0.5		1459.8	1297.7	*C,L*
		359.0	197.0	*C,L*
		616.4	454.5	*C,L*
		1635.7	1473.5	*C,L*
163.4±0.1	480±30	532.4	369.0	*C*,MR
164.0±0.5		454.5	290.5	*C,L*
		1151.2	987.2	*C,L*
165.8±0.1	29±4	987.2	821.8	*C,L*
		1495.0	1329.4	*C,L*
		1126.0	960.5	*C*
		885.8	720.3	*C*
167.5±0.5	780±40	850.2	682.7	*C,L*
168.0±0.1		338.8	170.7	*A,C*
		701.0	533.2	*C,L*
		1155.3	987.2	*C*
169.4±0.5		1214.7	1045.5	*C,L*
		891.9	722.0	*C*
170.4±0.3	~1	920.8	750.4	*C*
172.0±0.5	7±2	171.4	0	*C*
		1021.7	850.2	*C*
		1063.2	891.8	*C*
		1490.2	1318.5	*C*
		369.0	197.0	*C*
		722.0	550.4	*C*
172.9±0.5		682.7	509.8	*C,L*
174.8±0.2	11±2	1325.8	1151.2	*C*
		587.8	413.2	*C*
175.8±0.5	19±2	1473.5	1297.7	*C,L*
176.3±0.1		953.4	777.3	*C*
		661.1	485.0	*C*
		1325.8	1149.5	*C*
		1490.2	1314.2	*C*
179.4±0.5	30±10	1065.2	885.8	*C*
		225.4	46.2	*C*

TABLE I. (*Continued*).

Energy (keV)	Relative intensity	Assignment Initial level	Assignment Final level	Comments
180.8±0.5	44±5	471.3	290.5	*C*
181.5±0.5	70±10	987.2	805.9	*C*
		1063.2	881.5	*C*
183.5±0.5	73±10	960.5	777.3	*C*
		1065.2	881.5	*C*
		1107.2	923.3	*C*
184.9±0.5	5600±400	1250.9	1065.2	*C,L*
		801.0	616.4	*C,L*
185.7±0.5		1318.5	1133.0	*C*,MR
		793.8	608.0	*C*
		1250.9	1065.2	*C*
187.3±0.5	70±20	874.5	687.3	*C*
		1250.0	1063.2	*C*
		1646.8	1459.8	*C*
		413.2	225.4	*C*
189.5±0.1	770±40	438.6	249.1	*A,C*
		1390.5	1200.6	*C*
		911.7	722.0	*C*
		777.3	587.8	*C*
190.5±0.5		485.0	294.6	*C,L*
		1297.7	1107.2	*C,L*
		559.4	369.0	*C,L*
		664.5	474.1	*C,L*
		1151.2	960.5	*C,L*
191.7±0.5	3±1	881.5	690.2	*C*
		780.0	587.8	*C*
193.0±0.5	3±1	1214.7	1021.7	*C*
194.9±0.1	66±5	1155.3	960.5	*C*,PR
195.5±0.5		367.0	171.4	*C,A,L*
		1107.2	911.7	*C,L*
		1045.5	850.2	*C,L*
196.4±0.3	6±3	1149.5	953.4	*C*
		1329.4	1133.0	*C*
197.6±0.5	4±2	682.7	485.0	*C*
		805.9	608.0	*C*
199.5±0.5	3±1	1024.7	825.2	*C*
		1307.0	1107.2	*C*
200.9±0.2	55±4	920.8	720.2	*C*, mainly ^{234}U($8^+ \rightarrow 6^+$)
		559.4	359.0	*C*
		891.8	690.2	*C*
202.0±0.1	150±10	1155.3	953.4	*C*,PR
203.3±0.2	9±2	1235.2	1031.5	*C*
		874.5	671.1	*C*
		332.8	129.3	*C,A*
205.3±0.1	380±20	1250.9	1045.5	*C*,PR
		690.2	485.0	*C*
206.5±0.5	7±3	661.2	454.5	*C*
209.0±0.5	90±10	568.0	359.0	*C*

TABLE I. (*Continued*).

Energy (keV)	Relative intensity	Assignment Initial level	Assignment Final level	Comments
210.0±0.5	380±30	987.2	777.3	*C*
210.6±0.1		1235.2	1024.7	*C*, part. $^{238}U(8^+ \rightarrow 6^+)$
211.1±0.5	890±60	637.8	426.7	*C,L*
211.7±0.2		550.4	338.8	*A,C*
		780.0	568.0	*C*
213.2±0.5		874.5	661.1	*C,L*
		1063.2	850.2	*C,L*
		1235.2	1021.7	*C,L*
215.6±0.5	12±2	1065.2	850.2	*C*
		509.8	294.6	*C*
		885.8	670.9	*C*
		1107.2	891.8	*C*
217.1±0.5	~1	750.4	533.2	*C*
219.8±0.5	4±2	920.8	701.0	*C*
221.3±0.2	17±1	1456.8	1235.2	*C*,PR
222.0±0.5		1329.4	1107.2	*C,L*
		1473.5	1250.9	*C,L*
		1373.3	1151.2	*C,L*
224.1±0.5	15±5	1373.3	1149.5	*C*
		1473.5	1250.0	*C*
		1459.8	1235.2	*C*
225.7±0.5		225.4	0	*C,A*
		793.8	568.0	*C*
		1186.5	960.5	*C*
226.9±0.5	2±1	701.0	474.1	*C*
228.2±0.2	30±2	1021.7	793.8	*C*
		1151.2	923.3	*C*
		1250.0	1021.7	*C*
228.8±0.5		911.7	682.7	*C,L*
		587.8	359.0	*C,L*
230.9±0.1	15±2	891.8	661.1	*C*
232.5±0.1	300±20	671.1	438.6	*A,C*
232.5±0.5		1155.3	923.3	*C,L*
		687.3	454.5	*C,L*
		923.3	690.2	*C,L*
234.5±0.4	5±1	1647.0	1412.0	*C*,PR
		1297.7	1063.2	*C*
		793.8	559.4	*C*
235.7±0.5	~2	690.2	454.5	*C*
236.9±0.5	~1	1392.1	1155.3	*C*
		987.2	750.4	*C*
		722.0	485.0	*C*
237.8±0.5	15±2	664.5	426.7	*C,L*
		1149.5	911.7	*C,L*
238.5±0.1		1031.5	793.8	*C,L*
		1060.6	821.8	*C*,PR
		533.2	294.6	*C*
		1473.5	1235.2	*C*
239.4±0.5		608.0	369.0	*A,C,L*
		632.9	393.5	*C,L*
240.3±0.5	33±2	960.5	720.3	*C,L*
		1126.3	885.8	*C,L*
241.1±0.3		1392.1	1151.2	*C*

TABLE I. (*Continued*).

Energy (keV)	Relative intensity	Assignment Initial level	Assignment Final level	Comments
		1390.5	1149.5	*C*
		1133.0	891.8	*C*
		923.3	682.7	*C*
241.8±0.2	6±1	850.2	608.0	*C*
		413.2	171.4	*C*
		532.4	290.5	*C*
		1021.7	780.0	*C*
		801.0	559.4	*C*
242.7±0.5	3±1	533.2	290.5	*C*
243.4±0.2		1635.7	1392.1	*C*
244.3±0.1		1495.0	1250.9	*C*, part. ^{234}U($10^+ \rightarrow 8^+$)
		670.9	426.7	*C*
		777.3	533.2	*C*
	56±3	1126.3	881.5	*C*
		1024.7	780.0	*C*
		290.5	46.2	*C*, *A*
245.7±0.5		1635.7	1390.5	*C*, *L*
		471.3	225.4	*C*, *L*
		720.3	474.1	*C*, *L*
246.9±0.2	8±2	616.4	369.0	*C*, PR
248.8±0.5	7±3	608.0	359.0	*C*
		687.3	438.6	*C*
		474.1	225.4	*A*, *C*
250.2±0.3	11±2	920.8	670.9	*C*
		801.0	550.4	*C*
254.5±0.1		805.0	550.4	*A*, *C*
	280±20	1214.7	960.5	*C*
255.3±0.5		426.7	171.4	*A*, *L*
		1647.0	1392.1	*C*, *L*
		1490.2	1235.2	*C*, *L*
257.0±0.5		1647.0	1390.5	*C*, *L*
		825.2	568.0	*C*, *L*
257.8±0.2	210±10	1390.5	1133.0	*C*, mainly ^{238}U($10^+ \rightarrow 8^+$)
		1149.5	891.8	*C*
259.3±0.5		1065.2	805.9	*C*, *L*
261.3±0.5	~2	1214.7	953.4	*C*
262.1±0.3	~3	1063.2	801.0	*C*
		1325.8	1063.2	*C*
		1635.7	1373.2	*C*
263.1±0.2	16±2	953.4	690.2	*C*
264.2±0.3	~3	393.5	129.3	*A*, *C*
265.5±0.5	19±2	881.5	616.4	*C*, *L*
266.0±0.2		632.9	367.0	*C*
		1373.3	1107.2	*C*
		369.0	103.1	*C*, *A*
		1297.7	1031.5	*C*
		953.4	687.3	*C*
267.2±0.3	5±2	987.2	720.3	*C*
		777.3	509.8	*C*

TABLE I. (*Continued*).

Energy (keV)	Relative intensity	Assignment Initial level	Assignment Final level	Comments
268.2±0.4	~1	1045.5	777.3	*C*
269.7±0.2	11±3	1063.2	793.8	*C*
		682.7	413.2	*C*
270.9±0.5	5±2	953.4	682.7	*C*
271.4±0.4		664.5	393.5	*C*
272.8±0.5		1473.5	1200.6	*C,L*
		1297.7	1024.7	*C,L*
		805.9	533.2	*C,L*
273.8±0.2	210±10	944.9	671.1	*C*
		881.5	608.0	*C*
		805.9	532.4	*C*
274.5±0.5		720.3	445.7	*C,L*
275.3±0.3	3±1	1149.5	874.5	*C*
276.7±0.5	9±4	750.4	474.1	*C*
		474.1	197.0	*C*
		1126.3	850.2	*C*
277.6±0.2	20±2	616.4	338.8	*C*
		960.5	682.7	*C*
279.2±0.2	10±2	1412.0	1133.0	*C*
		750.4	471.3	*C*
280.3±0.5	2±1	1325.8	1045.5	*C*
283.6±0.3	4±2	454.5	170.7	*C*
		413.2	129.3	*C*
		1063.2	780.0	*C*
		1390.5	1107.2	*C*
		532.4	249.1	*C*
285.6±0.3	5±2	1307.0	1021.7	*C*
287.5±0.5	10±2	1065.2	777.3	*C*
		1318.5	1031.5	*C*
		701.0	413.2	*C*
289.2±0.5	2±1	1314.2	1024.7	*C*
		1200.6	911.7	*C*
291.8±0.5	~1	1097.7	805.9	*C*
293.9±0.3	7±2	1325.8	1031.7	*C*
		881.9	587.8	*C*
		1495.0	1200.6	*C*
295.4±0.1	180±9	1100.4	805.0	*C*
		911.7	616.4	*C*
		780.0	485.0	*C*
296.6±0.5		1250.0	953.4	*C,L*
		805.9	509.8	*C,L*
297.9±0.5	~2	885.8	587.8	*C*
300.0±0.1	20±2	471.3	171.4	*C*
300.6±0.1	100±20	1151.2	850.2	*C*, part. $^{238}U(12^+ \rightarrow 10^+)$
		471.3	170.7	*C*
304.0±0.5	11±2	1325.8	1021.7	*C,L*
305.0±0.3		1456.8	1151.2	*C*
		1126.3	821.8	*C*
		1186.5	881.9	*C*
		1155.3	850.2	*C*
		750.4	445.7	*C*

TABLE I. (*Continued*).

Energy (keV)	Relative intensity	Assignment Initial level	Assignment Final level	Comments
306.7±0.5	3±1	1635.7	1329.4	
		1456.8	1149.5	*C*
309.0±0.5	3±1	780.0	471.3	*C*
310.1±0.2	9±1	1060.6	750.4	*C*
		1459.8	1149.5	*C*
		1373.3	1063.2	*C*
		559.4	249.1	*C*
		413.2	103.1	*C*
311.6±0.2	17±2	393.5	81.8	*C*
		821.8	509.8	*C*
312.7±0.1	120±4	1257.5	944.9	*C*
316.6±0.1	42±2	445.7	129.3	*C*, mainly ^{234}U($14^+ \rightarrow 12^+$)
318.0±0.5	4±1	1647.0	1329.4	*C*
320.2±0.5	5±1	1126.3	805.9	*C*,*L*
		1097.7	777.3	*C*,*L*
321.3±0.1		1635.7	1314.2	*C*
		367.0	46.2	
322.3±0.5		661.1	338.8	*C*,*L*
326.8±0.5	~3	1459.8	1133.0	*C*
333.5±0.1	80±3	1214.7	881.5	*C*
		1433.9	1100.4	*C*
		332.8	0	*A*
336.6±0.3	7±1	1186.5	850.2	*C*
337.4±0.5		1024.7	687.3	*C*,*L*
338.0±0.5	62±8	1250.0	911.7	*L*
		1039.3	701.0	*C*,*L*
		509.8	171.4	*C*,*L*
338.8±0.1		1250.9	911.7	*C*, part. ^{238}U($14^+ \rightarrow 12^+$)
340.6±0.4	3±1	1060.6	720.3	*C*
348.5±0.2	43±2	1606.0	1257.5	*C*, part. ^{234}U($16^+ \rightarrow 14^+$)
		1126.3	777.3	*C*
		1373.3	1024.7	*C*
		687.3	338.8	
352.3±0.2	9±1	1459.8	1107.2	*C*
		911.7	559.4	
359.6±0.2	10±2	1060.6	701.0	*C*
362.8±0.5	2±1	1045.5	682.7	*C*
363.7±0.3	2±1	1024.7	661.1	*C*
364.5±0.3	2±1	1214.7	850.2	*C*
367.1±0.3	7±1	1392.1	1024.7	*C*
		367.0	0	*A*
		413.2	46.2	
		616.4	249.1	*C*
368.2±0.2	31±2	1802.1	1433.9	*C*
		1039.3	670.9	*C*
		701.0	332.8	*C*
		471.3	103.1	
371.2±0.5	3±1	1151.2	780.0	*C*
372.5±0.3	24±2	960.5	587.8	*C* part. ^{238}U($16^+ \rightarrow 14^+$)
		1325.8	953.4	*C*

TABLE I. (*Continued*).

Energy (keV)	Relative intensity	Assignment Initial level	Assignment Final level	Comments
375.1±0.2	12±2	426.7	51.7	*A,C*, part. $^{234}U(18^+ \rightarrow 16^+)$
		1155.3	780.0	*C*
376.0±0.4	~2	1126.3	750.4	*C*
377.5±0.5	10±2	1097.7	720.2	*C,L*
379.3±0.2		911.7	532.4	*C*
380.7±0.2	17±2	1986.7	1606.0	*C*
		1186.5	805.9	*C*
		509.8	129.3	*C*
		393.5	13.0	*A,C*
382.1±0.3	~2	533.4	151.0	*A*
		1065.2	682.7	*C*
383.3±0.5	5±3	750.4	367.0	*C*
387.8±0.2	7±1	682.7	294.6	
389.7±0.5	~3	1060.6	670.9	*C*
392.7±0.4	6±2	682.7	290.5	*C*
		1214.7	821.8	*C*
		805.9	413.2	
		474.1	81.8	*A*
393.5±0.4	~3	393.5	0.1	*A*
		953.4	559.4	*C*
395.7±0.4	4±1	1647.0	1250.9	*C*
		690.2	294.6	
		1060.6	664.5	*C*
		1200.6	805.0	*C*
399.4±0.2	17±1	2201.5	1802.1	*C*
		445.7	46.2	
		987.2	587.8	*C*
		1200.6	801.0	*C*
401.5±0.5	2±1	1039.3	637.8	*C*
402.4±0.3	8±1	1325.8	923.3	*C*, part. $^{238}U(18^+ \rightarrow 16^+)$
		1063.2	661.1	*C*
406.1±0.4	5±1	1039.3	632.9	*C*
		1126.3	720.3	*C*
407.3±0.6	12±1	891.8	485.0	*C*
408.2±0.5	3±1	1024.7	616.4	*C*
409.0±0.4	6±2	2395.6	1986.7	*C*
		1214.7	805.9	*C*
		1186.5	777.3	*C*
410.4±0.3	3±1	881.5	471.3	
411.2±0.5	5±2	1647.0	1235.2	*C*
		608.0	197.0	*A,C*
		1133.0	722.0	*C*
		920.8	509.8	
		780.0	369.0	*C*
413.9±0.3	9±1	1459.8	1045.5	
		426.7	13.0	*A*
		413.2	0	

TABLE I. (*Continued*).

Energy (keV)	Relative intensity	Assignment Initial level	Assignment Final level	Comments
415.5±0.3	2±1	1307.0	891.8	*C*
416.6±0.3	~3	587.8	171.4	*C*
417.5±0.5		587.8	170.7	*C*
421.4±0.4	5±1	1307.0	885.8	*C*
		1214.7	793.8	*C*
		780.0	359.0	*C*
		953.4	532.4	*C*
422.6±0.3	5±1	474.1	51.7	*A*
		1060.6	637.8	
425.1±0.3	8±1	1456.8	1031.5	*C*
		1126.3	701.0	*C*
		1307.0	881.5	
		471.3	46.2	
426.6±0.3	7±1	1097.7	670.9	*C*
		911.7	485.0	*C*
		2628	2201.5	*C*
		881.5	454.5	*C*
		426.7	0.1	*A*
427.8±0.3	7±1	1459.8	1031.5	part. ^{238}U($20^+ \rightarrow 18^+$)
		509.8	81.8	
		1149.5	722.0	*C*
		1060.6	632.9	
429.2±0.4	4±1	532.4	103.1	
433.3±0.5	7±1	1097.7	664.5	*C,L*
434.8±0.3		1456.8	1021.7	*C*
		2830	2395.6	*C*
		793.8	359.0	*C*
436.4±0.4	2±1	874.5	438.6	*C*
437.1±0.5		1214.7	777.3	*C*
		805.9	369.0	*C*
438.2±0.3	3±1	687.3	249.1	
		1459.8	1021.7	
439.5±0.3	6±1	1314.2	874.5	*C*
445.7±0.2	18±2	616.4	170.7	
		445.7	0	*C*
		1390.5	944.9	
446.8±0.5	~2	1063.2	616.5	
451.6±0.4	4±2	533.2	81.8	*A*
456.9±0.4	~3	608.0	151.0	*A,C*
		911.7	454.5	*C*
		682.7	225.4	*C*
		1024.7	568.0	*C*
		1307.0	850.2	
459.8±0.5	~3	750.4	290.5	*C*
		1097.7	637.8	*C*
463.8±0.3	5±1	1031.5	568.0	*C*
		509.8	46.2	*C*
465.3±0.5	2±1	1024.7	559.4	*C*
468.5±0.5	3±1	953.4	485.0	*C*
472.2±0.3	9±5	1297.7	825.2	*C*

TABLE I. (*Continued*).

Energy (keV)	Relative intensity	Assignment Initial level	Assignment Final level	Comments
473.4±0.4	3±2	911.7	438.6	
475.4±0.3	4±2	701.0	225.4	*C*
489.0±0.5	2±1	1314.2	825.2	*C*
493.0±0.3	6±1	1126.3	632.9	
		690.2	197.0	
		1297.7	805.0	
		1318.5	825.2	*C*
		664.5	171.4	
495.2±0.5	3±1	1063.2	568.0	*C*
508.5±0.5		637.8	129.3	*C*
509.5±0.5		509.8	0	*C*
		1314.2	805.0	*C*
511.8±0.5		682.7	170.7	*C*
512.9±0.5		1235.2	722.0	*C*
		1063.2	550.4	*C*
522.9±0.5	4±2	881.5	359.0	*C*
529.6±0.5	4±2	701.0	171.4	*C*
532.0±0.5	4±2	682.7	151.0	*C*
535.5±0.5	4±2	664.5	129.3	*C*
536.5±0.5	5±2	1021.7	485.0	*C*
539.2±0.3	9±2	690.2	151.0	*C*
		1107.2	568.0	
		1200.6	661.1	*C*
540.5±0.4	12±2	1647.0	1107.2	*C*
545.0±0.5	6±2	1490.2	944.9	*C*
550.6±0.6	7±2	1495.0	944.9	
552.9±0.3	10±2	911.7	359.0	
		750.4	197.0	
		891.8	338.8	
555.8±0.2	27±9	850.2	294.6	
557.1±0.3	12±2	1107.2	550.4	*C*
		805.9	249.1	
563.8±0.6	5±1	1235.2	671.1	
		1097.7	533.2	
		923.3	359.0	*C*
569.5±0.3	14±2	720.3	151.0	*C*
571.7±0.5	4±2	701.0	129.3	*C*
579.4±0.5	20±5	1250.9	671.1	
		750.4	170.7	
		682.7	103.1	*C*
580.3±0.5		777.3	197.0	*C*
583.2±0.5	32±3	1133.0	550.4	*C*
		1151.2	568.0	
		780.0	197.0	
		1021.7	438.6	*C*
		664.5	81.8	
584.6±0.5	20±2	923.3	338.8	*C*
		1459.8	874.5	
586.2±0.6	10±2	1060.6	474.3	
		1390.5	805.0	
		637.8	51.7	
		1024.7	438.6	
587.2±0.5	5±2	1392.1	805.0	*C*
588.8±0.5	5±2	1250.0	661.1	*C*

TABLE I. (*Continued*).

Energy (keV)	Relative intensity	Assignment Initial level	Assignment Final level	Comments
592.9±0.5	~2	1126.3	533.2	*C*
595.9±0.4	11±3	1155.3	559.4	*C*
597.9±0.4	28±5	1214.7	616.4	
		701.0	103.1	*A,C*
599.5±0.4	11±5	750.4	151.0	
		1149.5	550.4	
601.1±0.4	18±5	850.2	249.1	*A,C*
		1151.2	550.4	
		960.5	359.0	
606.7±0.5	28±3	1045.5	438.6	
		1329.4	722.0	*C*
		1214.7	608.0	
		1412.0	805.0	*C*
		777.3	170.7	*A*
609.1±0.5	16±2	780.0	170.7	*C*
		805.9	197.0	
610.9±0.4	3±1	1065.2	454.5	*C*
612.8±0.4	22±2	1039.3	426.7	
		664.5	51.7	
614.4±0.4	16±2	953.4	338.8	*C*
617.1±0.4	49±4	720.3	103.1	*A,C*
		1307.0	690.2	
		911.7	294.6	*C*
618.3±0.4	56±5	664.5	46.2	*A*
		987.2	369.0	*C*
619.2±0.4	17±5	670.9	51.7	*C*
		701.0	81.8	
619.8±0.4	15±5	632.9	13.0	
		1307.0	687.3	
622.3±0.6	7±3	1107.2	485.0	*C*
		960.5	338.8	
		793.5	170.7	
623.5±0.5 624.7±0.2	103±6	1097.7	474.1	*C,L*
		821.8	197.0	*C*
		670.9	46.2	*A,C*
		637.8	13.0	
		1063.2	438.6	
626.4±0.2	6±2	777.3	151.0	
		1297.7	671.1	*C*
630.4±0.4	16±2	920.8	290.5	*C*
632.9±0.2	130±20	632.9	0	*A,C*
		881.5	249.1	*C*
		1200.6	568.0	*C*
635.1±0.5	23±2	805.9	170.7	*C*
637.7±0.2	180±10	637.8	0	*A*
642.6±0.5	7±1	891.8	249.1	
		1314.2	671.1	
645.8±0.3	10±2	1039.3	393.5	
647.2±0.3	24±3	750.4	103.1	
		1318.5	671.1	

TABLE I. (*Continued*).

Energy (keV)	Relative intensity	Assignment Initial level	Assignment Final level	Comments
649.2±0.5	11±2	701.0	51.7	
650.1±0.3	6±2	1200.6	550.4	*C*
651.6±0.5	18±2	821.8	170.7	*C*
		1126.3	474.1	*C*
		1456.8	805.0	
		664.6	13.0	
654.8±0.3	41±4	1126.0	471.3	*C*
		805.9	151.0	*C*
		701.0	46.2	*A,C*
655.5±0.5		1456.8	801.0	*C,L*
658.7±0.4	13±2	953.4	294.6	
		1459.8	801.0	*C*
		1329.4	671.1	*C*
662.6±0.5	5±2	911.7	249.1	*C*
664.5±0.3	40±3	1490.2	825.2	*C*
		1325.8	661.1	*C*
		1149.5	485.0	*C*
		664.6	0	*A*
668.9±0.5	12±2	1107.2	438.6	
		750.4	81.8	*C*
		1390.5	722.0	
		1473.5	805.0	
670.0±0.5	24±3	1495.0	825.2	*C,L*
670.9±0.3		670.9	0	*A,C*
		821.8	151.0	*C*
		1097.7	426.7	
674.1±0.3	50±4	720.3	46.2	*A*
		777.3	103.1	*A,C*
		923.3	249.1	*C*
679.7±0.4	16±3	850.2	170.7	*C*
683.0±0.5	40±10	1250.9	568.0	*C,L*
684.8±0.3		1235.2	550.4	*C*
		1490.2	805.0	
		1097.7	413.2	*C*
		881.5	197.0	*C*
685.9±0.5	6±2	1024.7	338.8	*C*
693.0±0.5	15±5	1031.5	338.8	*C*
700.6±0.3	12±3	1250.9	550.4	
702.6±0.3	28±3	805.9	103.1	
		1373.3	671.1	*C*
		1647.0	944.9	
704.1±0.3	21±3	1063.2	359.0	*C*
		750.4	46.2	
		953.4	249.1	
706.5±0.5	~1	1045.5	338.8	*C*
709.1±0.5	2±1	1325.8	616.4	
712.2±0.4	2±1	1151.2	438.6	
715.3±0.5	4±2	885.8	170.7	*C*
		1186.5	471.3	
		1200.6	485.0	
719.1±0.4	4±2	821.8	103.1	*A*
		1390.5	671.1	

TABLE I. (*Continued*).

Energy (keV)	Relative intensity	Assignment Initial level	Assignment Final level	Comments
724.4±0.4	2±1	1063.2	338.8	*C*
726.7±0.3	3±1	1065.2	338.8	*C*
728.2±0.4	2±1	1060.6	332.8	*C*
730.2±0.5	5±1	1097.7	367.0	
		1297.7	568.0	*C*
734.4±0.3	5±1	885.8	151.0	
		1456.8	722.0	*C*
737.5±0.5	4±1	987.2	249.1	*C*
		1459.8	722.0	*C*
743.7±0.5	6±2	1214.7	471.3	
746.7±0.6	10±2	1297.7	550.4	*C*
		1314.2	568.0	
748.4±0.6	3±1	1307.0	559.4	*C*
760.0±0.5	~3	805.9	46.2	
		1214.7	454.5	
763.3±0.5	6±2	960.5	197.0	*C*
765.8±0.2	49±4	1250.9	485.0	*C*
768.1±0.4	12±2	1107.2	338.8	
		1318.5	550.4	*C*
773.0±0.4	6±1	1495.0	722.0	
		1021.7	249.1	
		1186.5	413.2	
775.9±0.3	10±5	821.8	46.2	*A*
		1325.8	550.4	
778.2±0.6	22±2	1329.4	550.4	
		881.5	103.1	*C*
782.7±0.3	12±2	885.8	103.1	*A*
		953.4	170.7	
790.3±0.5	7±2	960.5	170.7	*A,C*
796.4±0.4	10±2	1045.5	249.1	
		1235.2	438.6	
798.3±0.4	8±2	1459.8	661.1	
802.6±0.5	42±4	1473.5	671.1	
810.7±0.3	30±3	1149.5	338.8	
812.1±0.6	11±2	1151.2	338.8	
		1250.9	438.6	*C*
816.4±0.3	22±3	987.2	170.7	
		1065.2	249.1	*C*
		1155.3	338.8	*C*
817.8±0.4	23±3	920.8	103.1	*A*
		1186.5	369.0	
821.5±0.3	32±5	821.8	0	*A*
		1647.0	825.2	*C*
822.5±0.6	5±4	1307.0	485.0	
		1373.3	550.4	
839.6±0.5	29±3	885.8	46.2	*A*
		1390.5	550.4	*C*
849.8±0.4	25±3	953.4	103.1	
855.3±0.6	9±2	1214.7	359.0	*C*
857.9±0.6	20±4	960.5	103.1	*A*

TABLE I. (*Continued*).

Energy (keV)	Relative intensity	Assignment Initial level	Assignment Final level	Comments
		1107.2	249.1	
859.9±0.6	12±3	1297.7	438.6	
874.7±0.2	62±6	1045.5	170.7	*C*
		920.8	46.2	*A*
876.0±0.5		1214.7	338.8	*C*
887.1±0.4		1325.8	438.6	*C*
888.5±0.5		1456.8	568.0	*C*
894.3±0.5	17±2	1065.2	170.7	*C*
901.8±0.6	9±2	1151.2	249.1	
		1126.3	225.4	
906.0±0.5	7±2	1456.8	550.4	
		1155.3	249.1	
909.9±0.6	3±2	1459.8	550.4	
		1039.3	129.3	
911.1±0.6	12±3	1250.0	338.8	*C*
920.1±0.5	170±10	1214.7	294.6	*C,L*
920.8±0.2		920.8	0	*A*
925.4±0.5	11±1	1647.0	722.0	
926.4±0.5	12±2	1097.7	171.4	
935.4±0.6	5±1	1373.3	438.6	
941.2±0.2	37±3	987.2	46.2	*A*
948.3±0.5	9±2	1307.0	359.0	*C*
962.0±0.3	18±2	1065.2	103.1	*C*
964.4±0.5	5±2	1635.7	671.1	
968.8±0.5	11±2	1097.7	129.3	
		1307.0	338.8	
975.4±0.6	8±3	1647.0	671.1	
		1459.8	485.0	
		1126.3	151.0	
983.9±0.6	38±2	1155.3	170.7	*C*
994.7±0.4	6±1	1097.7	103.1	*C*
1000.9±0.3	6±1	1250.0	249.1	
1014.4±0.3	73±7	1060.6	46.2	*C*
1015.6±0.5	16±3	1097.7	81.8	
		1186.5	170.7	*C*
1019.0±0.6	7±3	1456.8	438.6	
1023.2±0.5	8±3	1126.3	103.1	
1039.4±0.5	15±5	1039.3	0	
1044.0±0.6	9±3	1214.7	170.7	
1051.7±0.6	6±2	1097.7	46.2	
1057.0±0.6	6±3	1307.0	249.1	
1060.5±0.5	13±2	1060.6	0	
1076.7±0.4	9±2	1325.8	249.1	
1083.2±0.6	4±1	1186.5	103.1	
1097.5±0.5	10±3	1097.7	0	
1111.9±0.3	9±2	1214.7	103.1	
1120.9±0.4	13±2	1459.8	338.8	
1126.3±0.5	6±3	1126.3	0	
1140.5±0.6	13±2	1186.5	46.2	

and 701 keV, as members of the $\frac{3}{2}^-$ $(K-2)$ γ-vibrational band based on the ground state. The arguments for such an assignment were mainly based on comparisons of experimental estimations and theoretical calculations of relative $B(E2)$ for the excitation and deexcitation of the three levels mentioned above. This interpretation was also confirmed by further experiments.[8,11]

In the present work, the rotational sequence in this

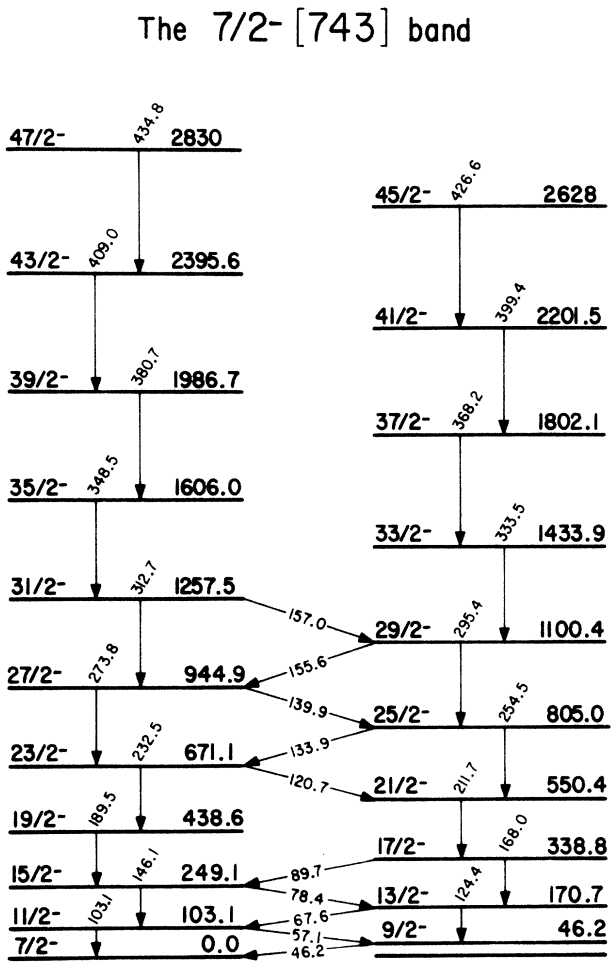

FIG. 5. The ground state $\frac{7}{2}^-[743]$ band of ^{235}U.

band has been proposed on the basis of the deexcitation modes toward seven different bands ($\frac{5}{2}^-[752]$, $\frac{7}{2}^-[743]$, $\frac{1}{2}^+[631]$, $\frac{3}{2}^+[631]$, $\frac{5}{2}^+[622]$, $\frac{5}{2}^+[633]$, and $\frac{7}{2}^+[624]$), and the population of the states from the $\frac{11}{2}^-\{\frac{7}{2}^-[743], 2_\gamma^+\}$ and $\frac{3}{2}^-\{[761]+[741]\}$ bands, lying at higher energy. With this set of transitions connecting the band to the others, and with the two intraband cascades (63.2, 104.9, 147.5, 196.1, 241.0 keV and 85.8, 131.6, 181.3, 234.5 keV corresponding to the two different signature sequences), we may propose the rotational sequence shown in Fig. 9 up to the $\frac{23}{2}^-$ state.

The predominant vibrational character of this band is in agreement with the fact that the moment of inertia is close to the ground band one ($\hbar^2/2J \sim 5.1$ keV). However, the similarity of the two bands is not complete. The energy spacings are roughly the same in both bands for the negative signature sequence (for example, the $\frac{11}{2}^- \rightarrow \frac{7}{2}^-$ transition energies are, respectively, 103.1 and 104.9 keV in the g.s. b and in the $\frac{3}{2}^-$ band; the $\frac{15}{2}^- \rightarrow \frac{11}{2}^-$ ones are, respectively, 146.1 and 147.5 keV). The situation is slightly different in the positive signature sequence where the $\frac{13}{2}^- \rightarrow \frac{9}{2}^-$ spacings have values of 124.4 and 131.6 keV, and the $\frac{17}{2}^- \rightarrow \frac{13}{2}^-$ spacings have values of 168.0 and

TABLE II. Coriolis mixing in the ground state $\frac{7}{2}^-[743]$ band: the standard basis element $\alpha \mid IMK\rangle$ is defined by the label $K^\pi[N,N_z,\Lambda]$ of the intrinsic state α on which it is built. Major weights are given in percent up to 95% of the state. For each state I of this band, the upper (lower) line in the table corresponds to the ^{234}U core (^{236}U core) calculation. Experimental value of the state energy is given on the central line.

State J	Energy (MeV)	$\frac{7}{2}^-[743]$ (%)	$\frac{5}{2}^-[752]$ (%)	$\frac{9}{2}^-[734]$ (%)
$\frac{7}{2}$	0.00	91	9	
	0.00			
	0.00	>95		
$\frac{9}{2}$	0.01	83	16	
	0.05			
	0.03	>95		
$\frac{11}{2}$	0.04	77	20	
	0.10			
	0.06	91	5	4
$\frac{13}{2}$	0.07	73	23	
	0.17			
	0.11	88	6	5
$\frac{15}{2}$	0.11	70	26	
	0.25			
	0.17	85	8	7
$\frac{17}{2}$	0.17	66	28	4
	0.34			
	0.23	82	9	8
$\frac{19}{2}$	0.24	63	30	4
	0.44			
	0.31	80	11	9
$\frac{21}{2}$	0.32	62	30	4
	0.55			
	0.40	77	12	10
$\frac{23}{2}$	0.41	59	32	5
	0.67			
	0.50	75	13	10
$\frac{25}{2}$	0.52	58	33	5
	0.80			
	0.62	73	14	11
$\frac{27}{2}$	0.62	55	34	5
	0.94			
	0.74	71	15	12
$\frac{29}{2}$	0.75	56	34	5
	1.10			
	0.87	70	15	12
$\frac{31}{2}$	0.87	53	35	5
	1.26			
	1.01	69	16	12

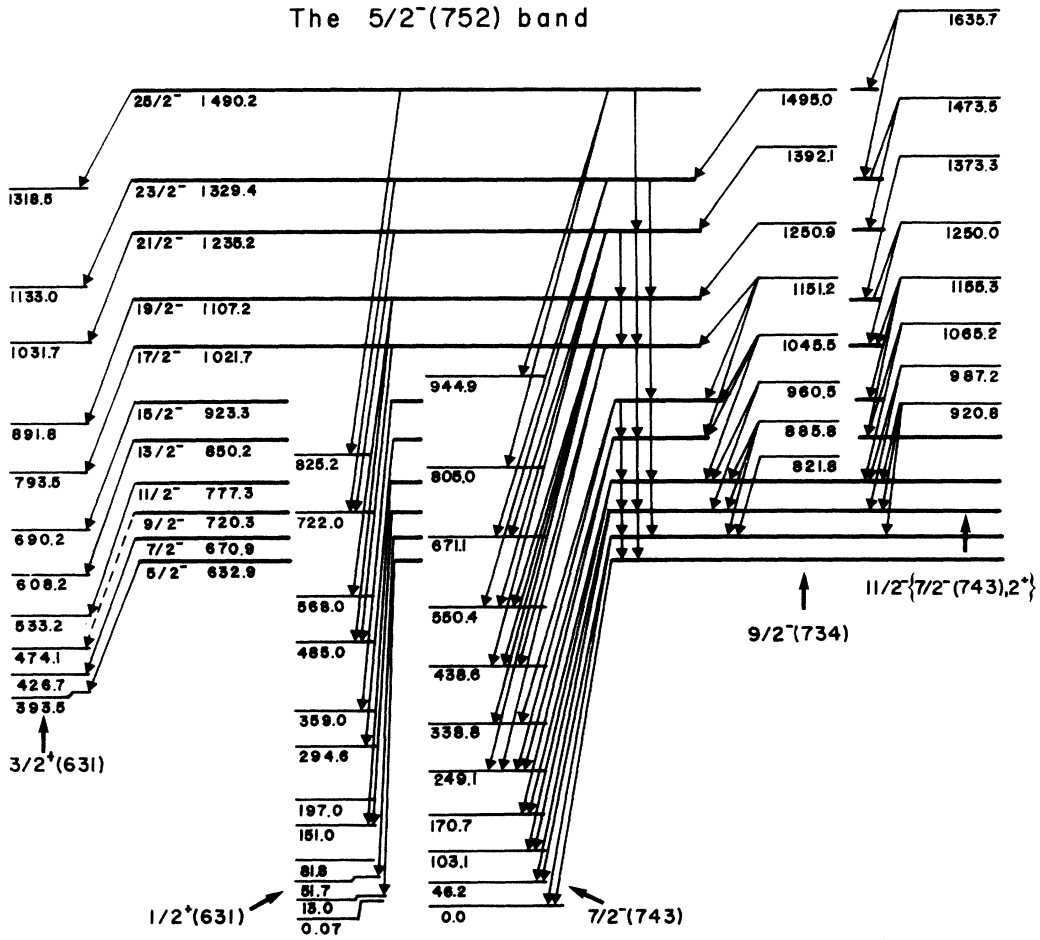

FIG. 6. The $\frac{5}{2}^-[752]$ band. For connections of this band with $\frac{3}{2}^-[761]$, $\frac{3}{2}^-\{\frac{7}{2}^-[743], 2^+\}$, and $\frac{7}{2}^+[624]$, see Figs. 8, 9, and 15, respectively. Note that because of the very large number of transitions, these are shown as arrows without mention of the energies which are found in Table I.

181.3 keV, respectively, in the ground and $\frac{3}{2}^-$ bands. In addition, the strong connections observed between this band and the $\frac{11}{2}^-$, suggested as the $(K+2)$ γ-vibrational band, are also in favor of the proposed interpretation.

However, the existence of a strong decay path from the other $\frac{3}{2}^-$ band lying at higher energy, which is assigned predominantly as $\frac{3}{2}^-\{[761]+[741]\}$ (see Sec. III A 4), indicates a possible admixture of single particle configurations.

6. The $\frac{11}{2}^-\{\frac{7}{2}^-[743], 2_\gamma^+\}$ band

The two first states, at 921 and 987 keV, have been previously identified.[4] The decay of each of these two levels is characterized by $E2$ transitions. The vibrational character of the band is strongly supported by the $B(E2)$ values. These levels have also been observed in (d,d') experiments.[12,13] In our Coulomb excitation experiments, this band has been excited up to the $\frac{25}{2}^-$ state at 1635.7 keV. As shown in Fig. 10, this band is connected mainly to the ground band and to the bands based on configurations closely related to the ground state one ($\frac{5}{2}^-[752]$, $\frac{9}{2}^-[734]$, and $\frac{3}{2}^-\{\frac{7}{2}^-[743], 2_\gamma^+\}$). A weaker decay is observed to the positive parity bands: $\frac{5}{2}^+[622]$ and $\frac{7}{2}^+[624]$. The energy spacings found in this band are very similar to those observed in the ground one.

B. The positive parity bands

1. The $\frac{1}{2}^+[631]$ band

The band head at 0.1 keV and the first members of this band have been identified and confirmed through various experiments (for a complete set of references, see Ref. 7). From the radioactive decay of ^{239}Pu the level energies up to $\frac{13}{2}^+$ at 294.6 keV have been accurately determined.[15] These results provide a good basis, which allowed us to extend this band up to the $\frac{23}{2}^+$ state at 825 keV (see Fig. 11).

It is difficult to establish from our results if this band is really populated by Coulomb excitation, because of its strong feeding from seven other bands. The decay of the $\frac{1}{2}^+[631]$ band states by intraband transitions and transi-

TABLE III. Electric and magnetic multipole properties in the $\frac{7}{2}^-[743]$ ground-state band. Experimental data are extracted, respectively, from Refs. 7, 38, and 39. The footnote c data stem from muonic x-ray fine structure studies. These data, concerning $I \rightarrow I + \Delta I$ transition probabilities are used here, by means of a suitable multiplication factor, for $I + \Delta I \rightarrow I$ transitions. Calculated value on the upper (lower) line of each part of the table corresponds to ^{234}U (^{236}U) core calculations. Magnetic moments are expressed in nuclear magnetons, μ_N, quadrupole moments in barns, and $E2$ reduced transition probabilities in $e^2\text{fm}^4$.

	Experimental value	Rotor-plus-qp theoretical values
Electric quadrupole moment of the $\frac{7}{2}^-$ ground state	4.55±0.09[a]	4.2
	4.1[a]	
	4.9[b]	4.6
Magnetic dipole moment of the $\frac{7}{2}^-$ ground state	−0.35[a]	−0.77
	−0.36[a]	
	−0.43[b]	−0.57
Intraband $E2$ reduced transition probability $B(E2, \frac{9}{2} \rightarrow \frac{7}{2})$	(3.868±0.013)×10^4[c]	4.0×10^4
		4.2×10^4
Intraband $E2$ reduced transition probability $B(E2, \frac{11}{2} \rightarrow \frac{7}{2})$	(0.7927±0.013)×10^4[c]	1.17×10^4
		1.10×10^4

[a]Reference 38.
[b]Reference 7.
[c]Reference 39.

tions to the ground band has been decisive for the identification of its high-energy members through γ-γ coincidences.

2. The $\frac{3}{2}^+[631]$ band

Previous studies by α decay of ^{239}Pu (see Refs. 15 and 16 and various reactions[13,17] led to the identification of the first members of this band up to the $\frac{11}{2}^+$ state at 608 keV. The multipolarities of the transitions deexciting the first three levels were also determined.[8]

As is shown in Fig. 12, we observe this band up to the $\frac{25}{2}^+$ state at 1412 keV. The band is strongly populated from the $\frac{3}{2}^-\{\frac{7}{2}^-[743], 2_\gamma^+\}$ and the $\frac{3}{2}^-\{[761]+[741]\}$ bands, while the feeding from the $\frac{5}{2}^-[752]$ is weaker. One observes a predominant decay of all the states of the band by one or several γ rays to those of the $\frac{1}{2}^+[631]$ band. Only the higher states of the band decay to the ground state band. A weaker decay is also observed to the $\frac{5}{2}^+[622]$ band. The intraband cascades are relatively strong. This band appears to be rather regular at low spin, while, with increasing spin, some irregularity takes place, reflecting a pronounced Coriolis mixing of the states.

3. The $\frac{5}{2}^+[622]$ band

This band has been observed up to the $\frac{19}{2}^+$ state at 661.1 keV. The first members ($I < \frac{13}{2}^+$) had been previously identified by several authors.[8,11,15] The multipolarity of a few transitions from the $\frac{5}{2}^+[633]$ and $\frac{3}{2}^+|631|$ bands to the band head at 129.3 keV has been measured as $M1$. This band has been proposed as the $\frac{5}{2}^+[622]$ one, using the information of its decay to the $\frac{1}{2}^+[631]$.[15] This assignment has been also confirmed through (d,p), (d,t), and (^{3}He,^{4}He) or (t,p) reactions.[11,14,17]

In the partial level scheme presented in Fig. 13, one may observe the feeding of this band from the $\frac{3}{2}^+[631]$, $\frac{5}{2}^+[633]$, and $\frac{7}{2}^+[624]$ bands, and also from the $\frac{3}{2}^-\{[761]+[741]\}$ and γ-vibrational $\frac{11}{2}^-$ and $\frac{3}{2}^-$ bands. This band decays to both ground and $\frac{1}{2}^+[631]$ bands. It is interesting to underline that it is connected to the $\frac{3}{2}^+[631]$ band which would be in favor of a $\frac{5}{2}^+[622]$ predominant configuration.

4. The $\frac{5}{2}^+[633]$ band

This band has been developed up to the $\frac{21}{2}^+$ state at 874.5 keV. The lowest part of the band was already proposed, up to the second $\frac{11}{2}^+$, by different ap-

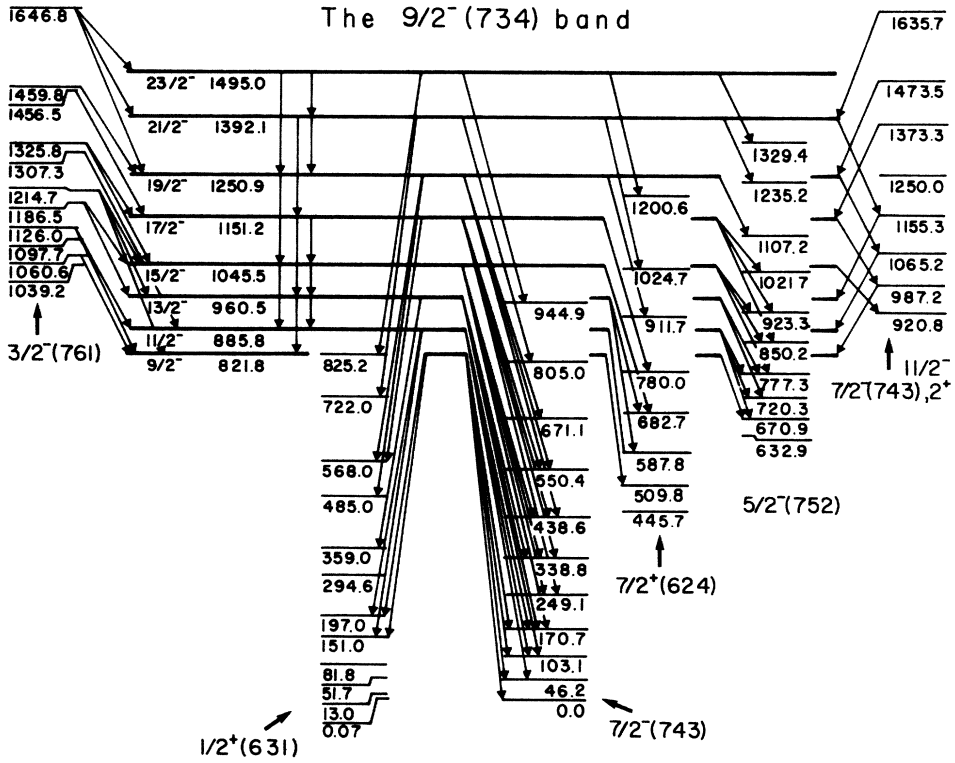

FIG. 7. The $\frac{9}{2}^-$[734] band. Same note as for Fig. 6.

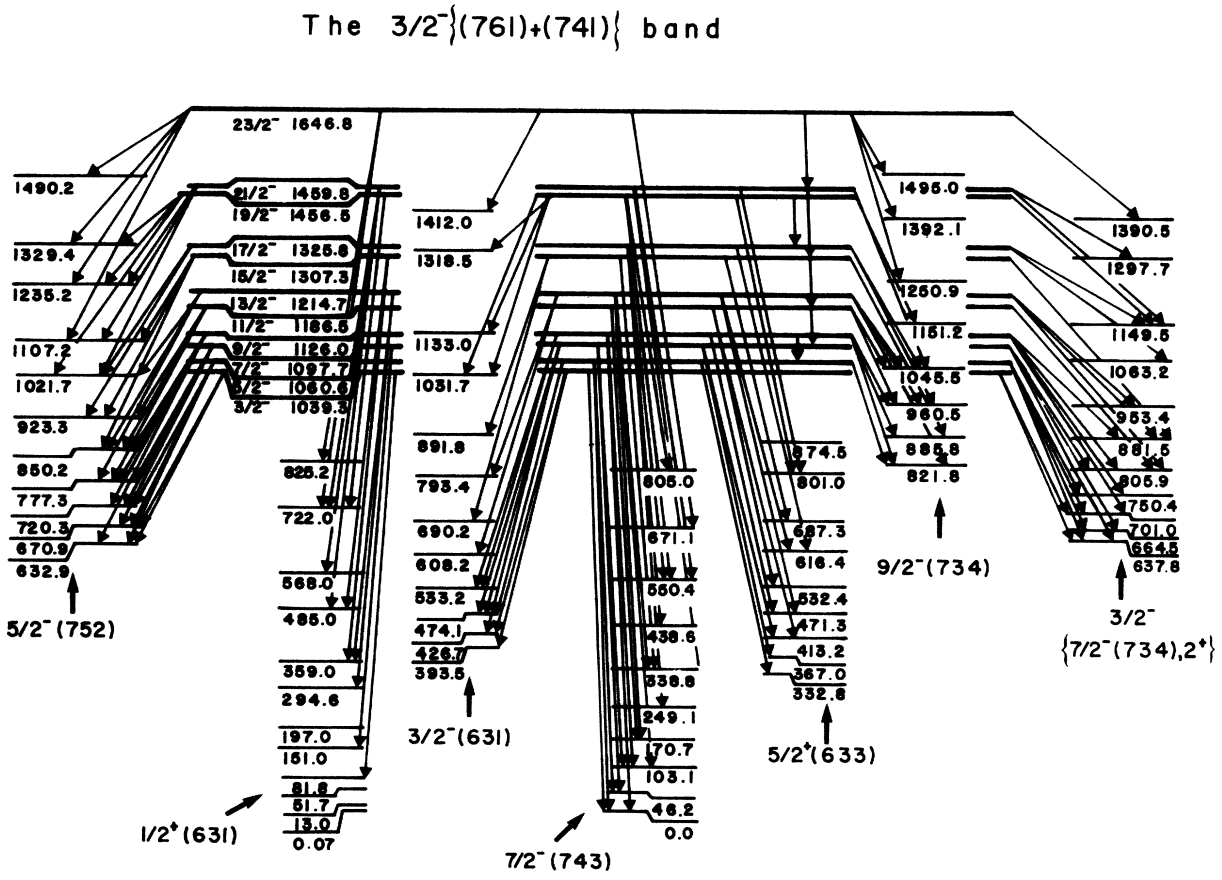

FIG. 8. The $\frac{3}{2}^-${[761]+[741]} band. For connections of this band with $\frac{5}{2}^+$[622], see Fig. 13. Same note as for Fig. 6.

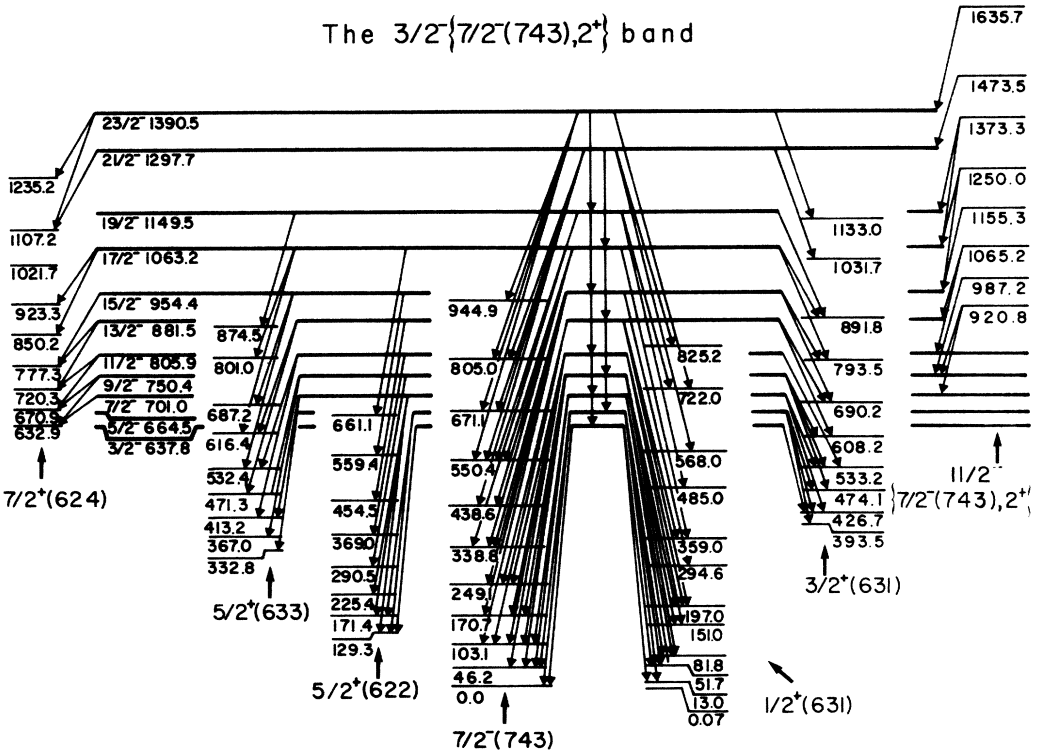

FIG. 9. The $\frac{3}{2}^-\{\frac{7}{2}^-[743], 2^+\}$ band. For connections of this band with $\frac{3}{2}^-[761]$ and $\frac{7}{2}^+[624]$, see Figs. 15 and 8, respectively. Same note as for Fig. 6.

proaches.[11,13,15,17] The multipolarities of the transitions deexciting the band head at 332.8 keV to different bands have been determined.[8]

The proposed level sequence shown in Fig. 14 contradicts a previous assignment of the $\frac{9}{2}^+$ level, which we place at 413.2 keV. These assignments within the band are based on the strong coincidences observed with the γ rays within the ground band up to the higher states. This band also strongly feeds the $\frac{5}{2}^+[622]$ band and receives an important flow from the $\frac{3}{2}^-\{[761]+[741]\}$, $\frac{3}{2}^-\{\frac{7}{2}^-[743], 2^+\}$, and $\frac{7}{2}^+[624]$ bands.

5. The $\frac{7}{2}^+[624]$ band

The first two or three states of this band were already proposed, but their interpretation remains doubtful.[8,13,14] In Ref. 14 the level at 509 keV was proposed as the $\frac{9}{2}^+$ state of a $\frac{7}{2}^+[624]$ band, while in Ref. 13 the three levels at 444, 510, and 585 keV were interpreted as the first members of an octupole band, $\frac{7}{2}^+\{\frac{7}{2}^-[743], 0^-\}$, based on the ground state. More recently, spin and parity $(\frac{7}{2}^+)$ of the 445.7 keV level have been determined through multipolarity measurements.[8] Through Coriolis mixing calculations, these authors concluded in favor of a mixing of $\frac{7}{2}^+\{\frac{7}{2}^-[743], 0^-\}$ and $\frac{7}{2}^+[624]$ configurations. From the present measurements, this band, whose band head is found at 445.7 keV, is observed up to the 1314 keV level, as shown in Fig. 15.

The states are populated by the $\frac{5}{2}^-[752]$, $\frac{9}{2}^-[734]$, $\frac{3}{2}^-\{\frac{7}{2}^-[743], 2^+\}$, and $\frac{11}{2}^-\{\frac{7}{2}^-[743], 2^+\}$ bands, while they decay mainly to the $\frac{5}{2}^+[622]$, $\frac{5}{2}^+[633]$, and $\frac{1}{2}^+[631]$ bands. One may notice that the decay of this $\frac{7}{2}^+$ band to the ground band is weak. These features may be used qualitatively to rule out the octupole configuration as the main component in this state. On the other hand, the $\frac{7}{2}^+[624]$ retained as the main component in our interpretation is well supported by our rotor-plus-quasiparticle calculations described in Sec. IV.

Finally, the observed rotational bands are summarized in Fig. 16.

IV. ROTOR-PLUS-QUASIPARTICLE APPROACH OF THE ^{235}U LEVEL SCHEME

The rotor-plus-quasiparticle model is *a priori* tailored for well deformed nuclei. The actinide region is therefore appropriate for such a model description. Under its crude but transparent assumptions, it yields the main behavior of these nuclei, as shown in a rotor-plus-quasiparticle approach using HF plus BCS single particle states[18] which has been recently applied to different regions of nuclei.[19–23] In Ref. 23 a brief description of the ^{235}U level scheme was included in a systematic study of heavy nuclei. In the present section such results are presented and compared to the completed spectroscopic data of ^{235}U in a more detailed way.

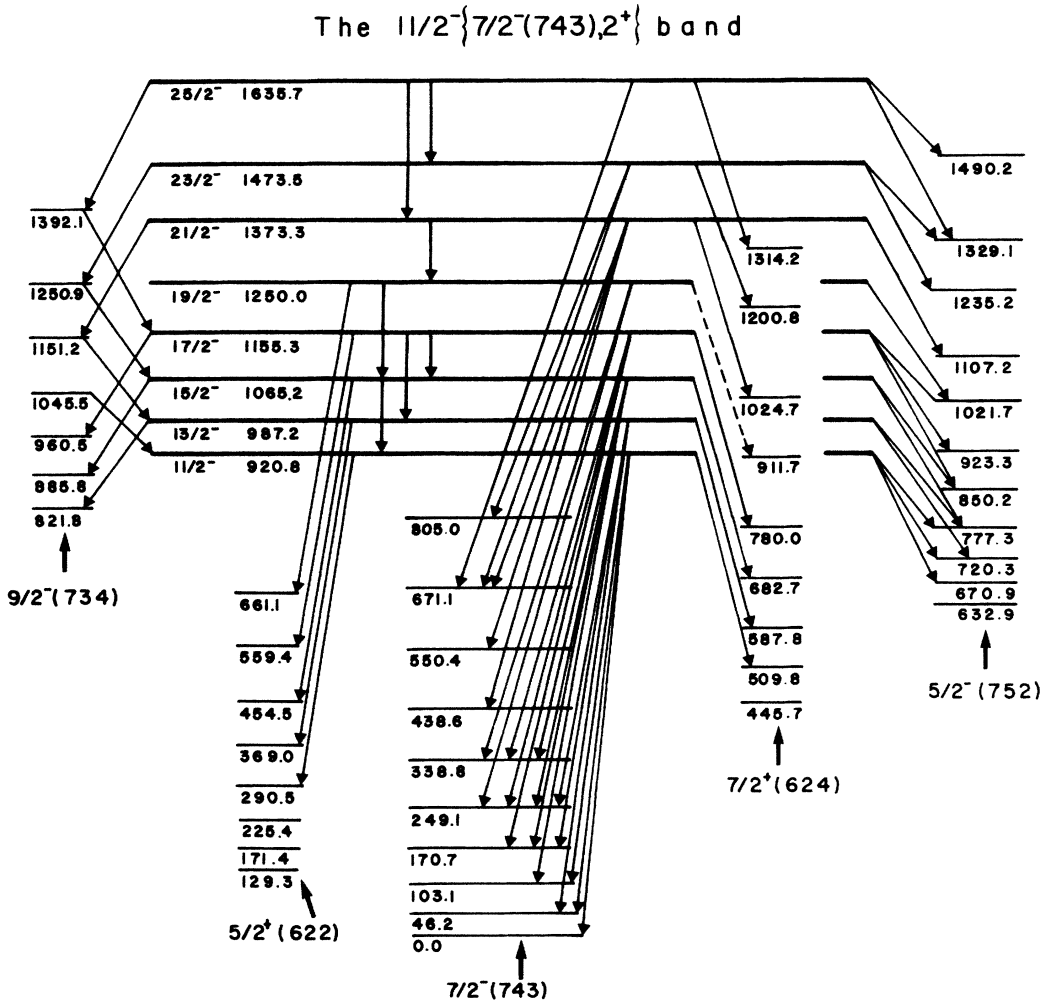

FIG. 10. The $\frac{11}{2}^-\{\frac{7}{2}^-[743], 2^+\}$ band. For connections of this band with $\frac{3}{2}^-\{\frac{7}{2}^-[743], 2^+\}$, see Fig. 9. Same note as for Fig. 6.

A. Brief survey of the method

As a preliminary step, the mean field corresponding to the two even-even cores ^{234}U,^{236}U is calculated. We make use of the Skyrme SIII effective force,[24] whose parameters have been fixed once for all, for the whole chart of nuclides. The HF plus BCS methods and numerical techniques have been described in Refs. 25–27. Let us recall, however, that we assume axial symmetry for the HF plus BCS solution and that the single states are expanded onto a truncated deformed oscillator basis including 13 major shells. Pairing effects are taken into account through an approximate BCS treatment[25,26] with pairing gaps deduced from experimental odd-even binding energy differences. The equilibrium HF plus BCS solution gives without any ambiguity the static deformation, which is therefore not to be considered a parameter of the model. As a first assessment of the quality of this approach, one would like to compare experimental and so-calculated bulk properties. As in many other regions of the nuclear chart (see Refs. 18, 24, 25 and 28–36), the binding energies in ^{234}U and ^{236}U are given after corrections, for truncation and 0^+ projection, within 1.5 MeV from experimental values.[36] Similarly, good agreement is also obtained for the static quadrupole moment, whose calculated values are, respectively, 9.88 and 10.07 b for these two nuclei, whereas corresponding experimental values are known to be 10.47 ± 0.05 and 10.80 ± 0.07 b.[37]

The HF plus BCS core calculations provide us with a set of one quasiparticle wave functions. A selection of one qp states in a range of ±4 MeV around the Fermi level is then introduced in the rotor-plus-qp Hamiltonian. For instance, ^{235}U is therefore described as a ^{234}U or as a ^{236}U core plus one quasiparticle neutron state. Both systems do not have the correct odd number of particles and can be understood as approximate but equivalent descriptions of the real odd nucleus. As shown in Fig. 17, we have thus selected about 20 quasiparticle states for each core labeled, as usual, by their main component on the deformed oscillator basis. However, it is important to stress that these states are often very much mixed by the HF Hamiltonian. Exact calculated weights on this basis, for ^{234}U and ^{236}U, can be found in Ref. 23.

The total Hamiltonian can then be written as

$$H = H_{\text{rot}} + H_{\text{intr}} ,$$

where the rotor kinetic energy is

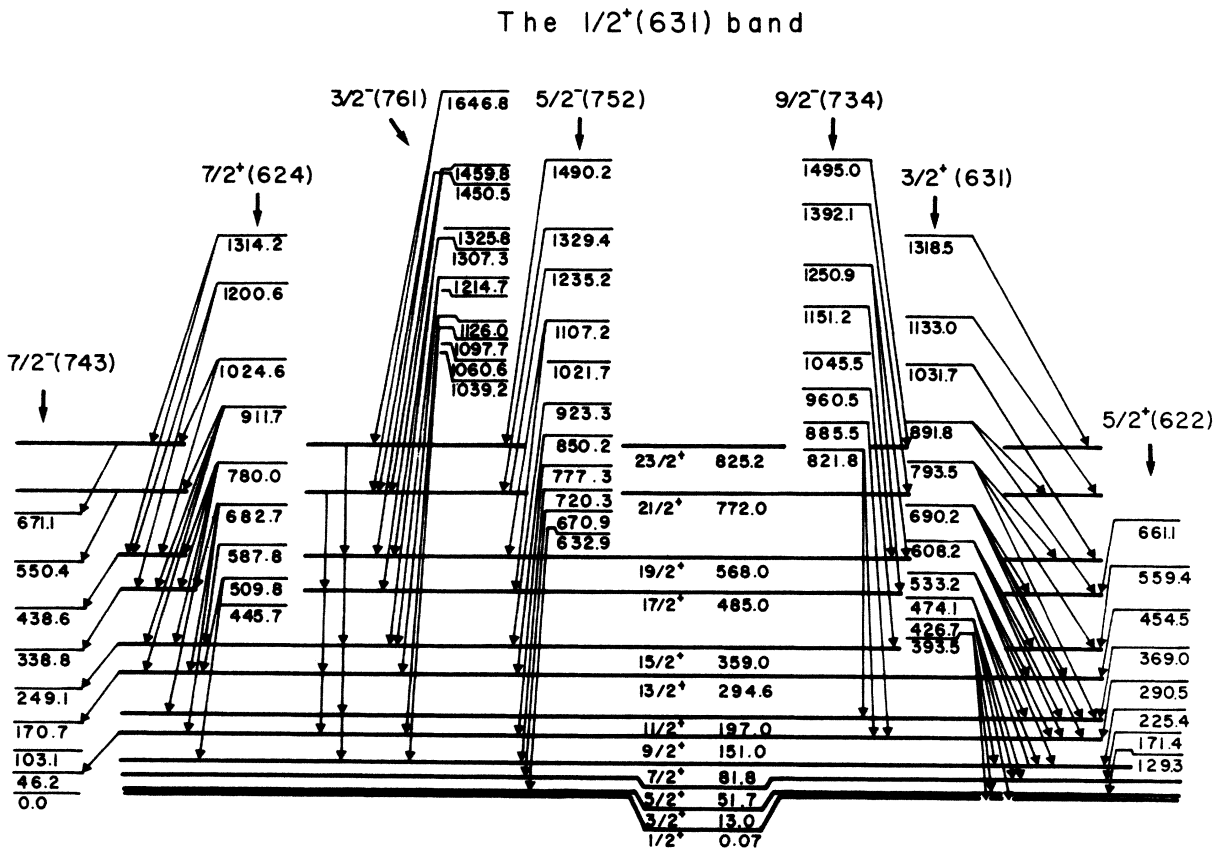

FIG. 11. The $\frac{1}{2}^+[631]$ band. For connections of this band with $\frac{3}{2}^-\{\frac{7}{2}^-[743], 2^+\}$, see Fig. 9. Same note as for Fig. 6.

$$H_{\text{rot}}=\frac{\hbar^2\mathscr{R}^2}{2J(R)} ,$$

$\mathscr{R}$ being the core angular momentum and R its eigenvalues in units of $\hbar$. This kinetic part has to reproduce the behavior of the even-even core, namely the experimental energies $E(R)$ of its ground state band. Thus, we introduce in the Hamiltonian these experimental even core energies, to obtain the corresponding variable moment of inertia:

$$J(R)=\frac{\hbar^2R(R+1)}{2E(R)} .$$

Under the assumption of axial symmetry ($R_z=0$), the total Hamiltonian is then fully determined: its intrinsic part through its solutions (i.e., the selected qp states) and its collective kinetic part through the above values for the moment of inertia. It thus appears that this Hamiltonian is not subject to any *ad hoc* adjustment, and is solved without any further approximation.

To deal with the R dependence of the moment of inertia, we perform the calculation of the matrix elements in the basis $|\alpha IMK\rangle$ (with the usual notation, where α contains the intrinsic quantum numbers) through an expansion onto eigenstates $|\beta IMjR\rangle$ of the core and of qp angular momenta, which implies a projection of the deformed qp states onto a spherically symmetrical basis. These projection techniques are described at length in Ref. 18. After diagonalization, one obtains the approximate odd-A nuclear states by their components onto the standard basis as

$$|\gamma IM\rangle=\sum_{\alpha K} C^{\gamma}_{\alpha K}\,|\alpha IMK\rangle .$$

Most of the resulting mixing comes from the so-called Coriolis term in the Hamiltonian. From these solutions one may calculate, as shown in Ref. 23, reduced $E2$ and $M1$ transition probabilities and associated moments.

B. Discussion of the results

In Fig. 18 the low spin part of rotational bands obtained in our Coulomb excitation measurements has been compared with the calculated ones. The discussion of results up to $I=\frac{31}{2}$ in the ground-state band and up to $I=\frac{21}{2}$ in the others is made through the following analysis, band by band.

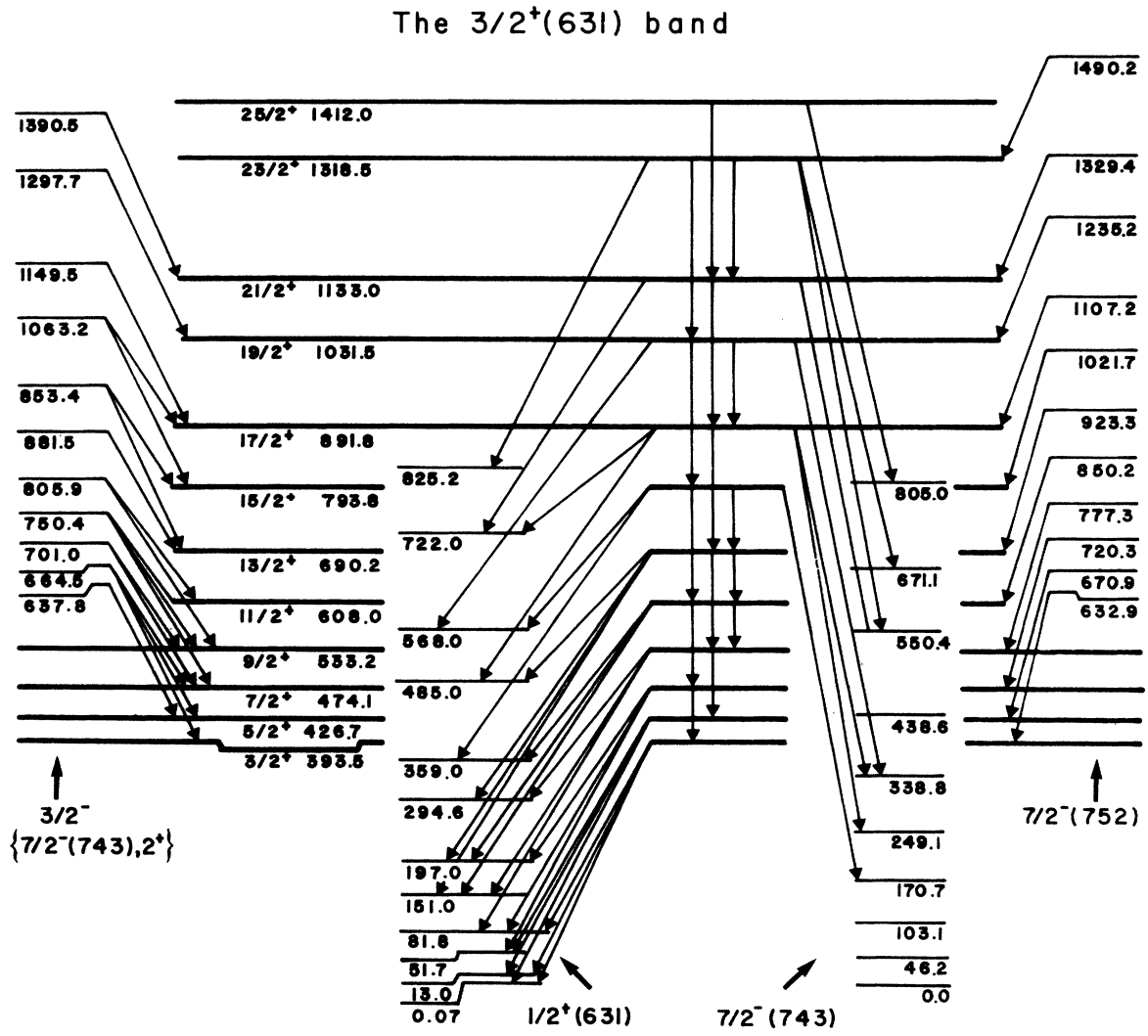

FIG. 12. The $\frac{3}{2}^+[631]$ band. For connections of this band with $\frac{5}{2}^+[622]$ and $\frac{3}{2}^-[761]$, see Figs. 13 and 8, respectively. Same note as for Fig. 6.

1. The $\frac{7}{2}^-[743]$ ground-state band

In the ^{234}U core calculation the pure $\frac{7}{2}^-[743]$ state is found to be the ground state. In the ^{236}U core calculation, this level, even though not the lowest in energy, appears only at 0.170 MeV above the lowest calculated state.

The experimental $\frac{7}{2}^-[743]$ assignment is thus in good agreement with our calculations. It should be noticed that, for the sake of coherence with Fig. 18, all energies extracted from the ^{236}U core calculation will be given as differences with the $\frac{7}{2}^-[743]$ states.

The calculations with both cores provide energy spacings smaller than the experimental ones. Insofar as this fact can be understood as an indication of Coriolis mixing between pure rotational bands, the calculated bands could exhibit an overestimated mixing behavior. This statement, however, should be quantitatively substantiated by the calculated mixing coefficients given in Table II, and which is found very low indeed, especially for the ^{236}U core calculations. One may remark that the Coriolis mixing is found stronger in the ^{234}U core calculations for most of the calculated bands, at moderate spin.

On the other hand, the experimental electric quadrupole and magnetic moments of the $\frac{7}{2}^-$ ground state and the $E2$ reduced transition probabilities within the ground-state band[7,38] are a very sensitive test of the theoretical description of the band. For these data, the agreement, as presented in Table III, is quite good, especially for such a description which does not enjoy any parameter adjustment.

2. The $\frac{5}{2}^-[752]$ band at 0.633 MeV

The experimental $\frac{5}{2}^-[752]$ band head is reproduced by both calculations (either too high or too low by several

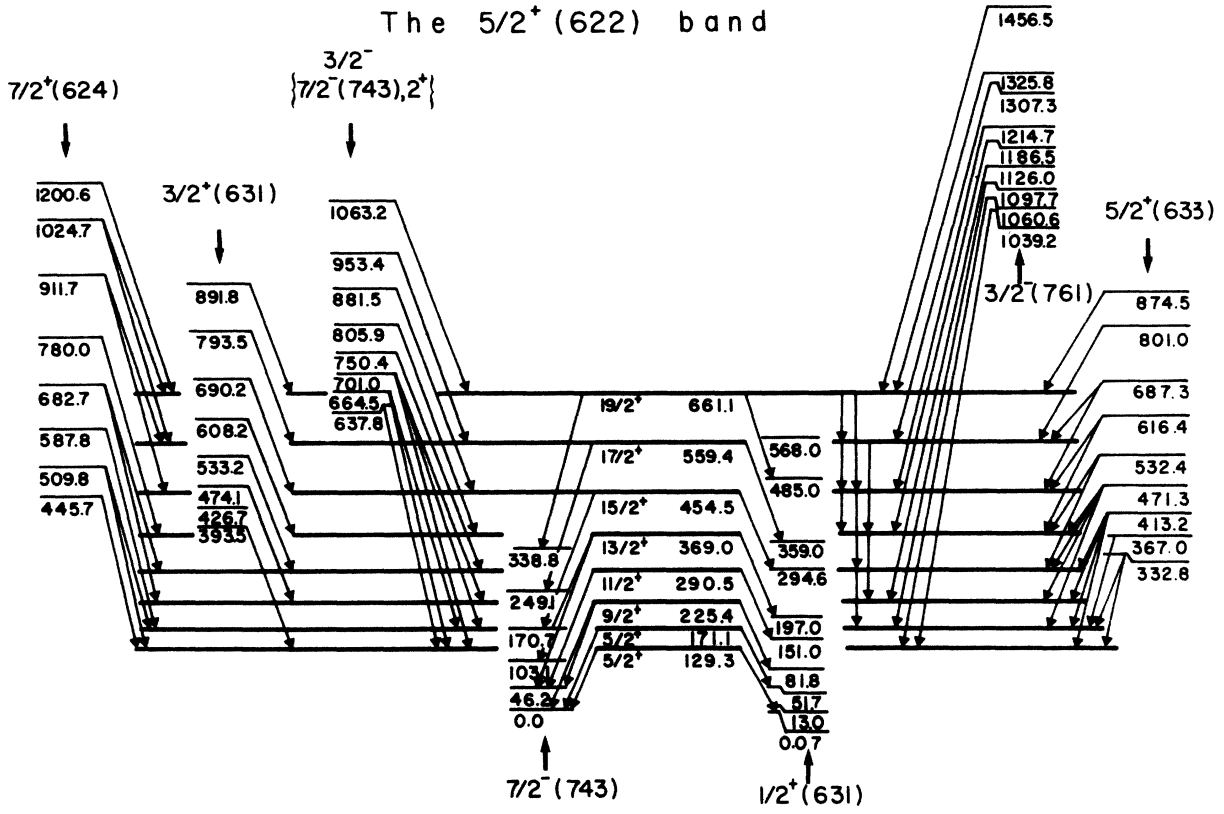

FIG. 13. The $\frac{5}{2}^+[622]$ band. For connections of this band with $\frac{11}{2}^-\{\frac{7}{2}^-[743], 2^+\}$, see Fig. 10. Same note as for Fig. 6.

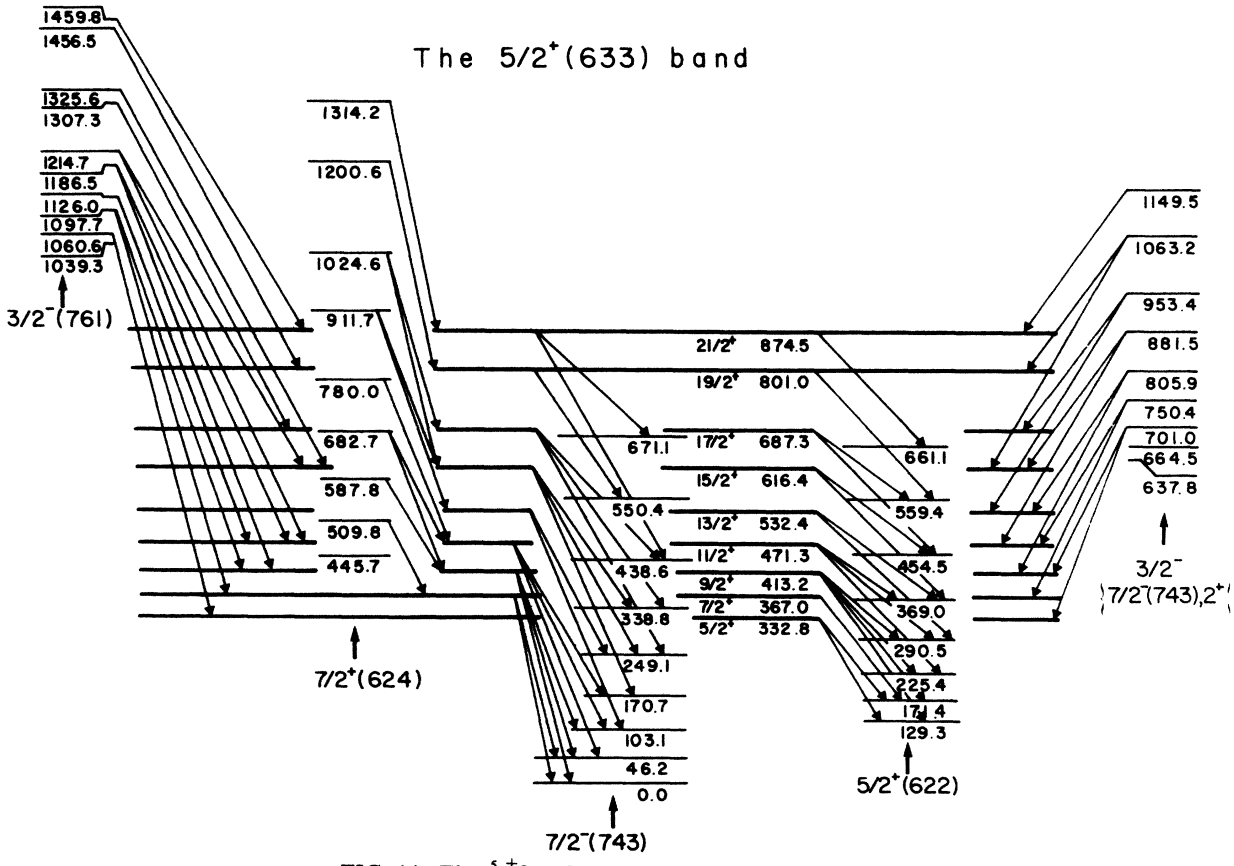

FIG. 14. The $\frac{5}{2}^+[633]$ band. Same note as for Fig. 6.

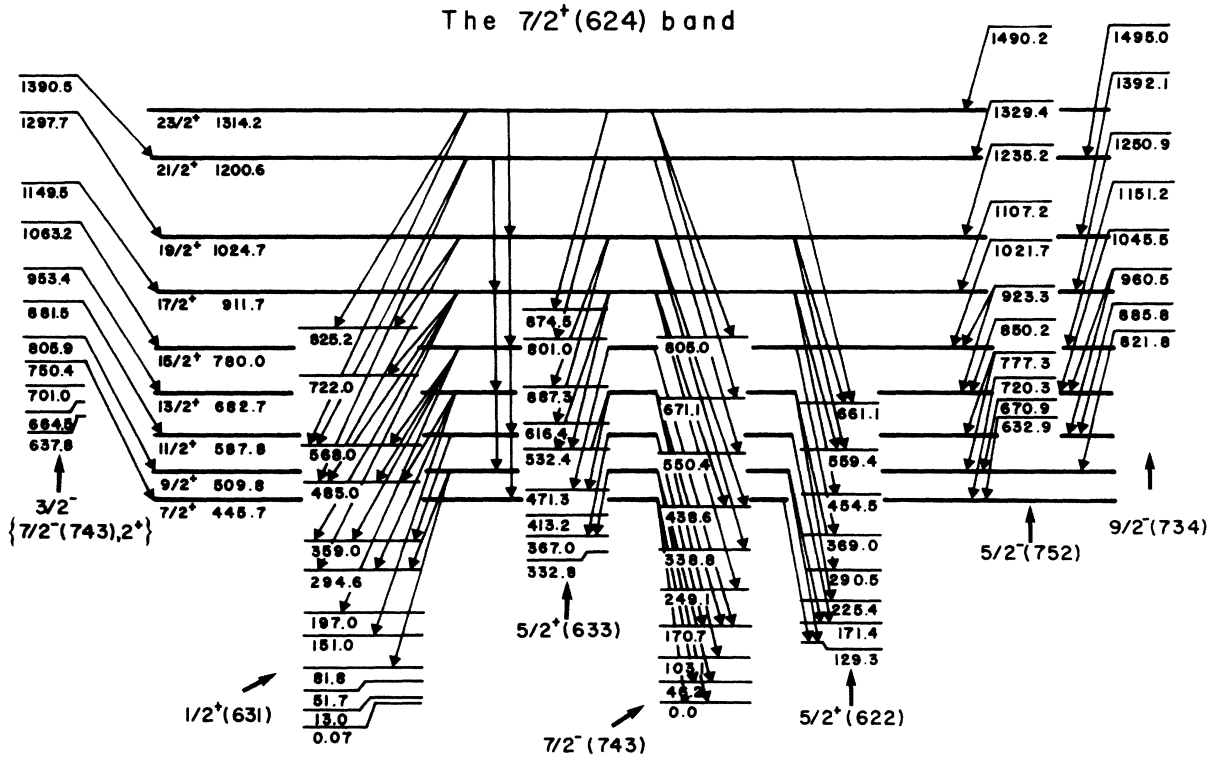

FIG. 15. The $\frac{7}{2}^+[624]$ band. For connections of this band with $\frac{11}{2}^-\{\frac{7}{2}^-[743], 2^+\}$, see Fig. 10. Same note as for Fig. 6.

hundred keV). This band has been already identified as $\frac{5}{2}^-[752]$, e.g., by Stephens *et al.*[4] through its connections with the ground-state band. These authors have measured $E2$ reduced transition probabilities from the ground state. Furthermore, relative $M1$ interband reduced transition probabilities to the ground-state band are also available. As shown in Table IV, calculations of these data confirm the identification of this band as based on the $\frac{5}{2}^-[752]$ state. Both calculations yield a slightly more perturbed character for this band, as observed experimentally (see Sec. III A 2). This band, almost pure in its lowest states, becomes strongly mixed (40—50% at $\frac{17}{2}$, ~80% at $\frac{25}{2}$), mainly with the $\frac{7}{2}^-[743]$ and $\frac{9}{2}^-[734]$ bands, and more weakly with the $\frac{3}{2}^-\{[761]+[741]\}$ band, which is in agreement with the observed favored connections.

3. The $\frac{9}{2}^-[734]$ band at 0.822 MeV

Both calculations yield this state within a compatible range of energy. The band-head energy is especially well reproduced in ^{236}U core calculations (0.88 instead of 0.82 MeV). The experimentally known interband $E2$ and $M1$ reduced transition probabilities have been reproduced in our calculations (see Table V) in such a way as to confirm the $\frac{9}{2}^-[734]$ assignment. Under this hypothesis, the analysis of Coriolis mixing shows that this band is significantly connected to the $\frac{3}{2}^-\{[741]+[761]\}$ band (in the ^{234}U core calculation) and even at very low spin to the $\frac{5}{2}^-[752]$ band (in the ^{236}U core calculation). This is to be compared with the previous given experimental observations concerning band connections.

4. The $\frac{3}{2}^-$ bands

The experimental information about the $\frac{3}{2}^-$ band heads in this nucleus may be summed up as follows:

(a) A first band head is observed at 0.638 MeV. Its corresponding band is very well developed in our Coulomb excitation measurements, and it has been proposed[4] as being based on a vibrational state $\frac{3}{2}^-\{[743], 2^+_\gamma\}$. We do not expect, of course, to reproduce it in our calculations.

(b) Another one has been observed at 0.806 MeV in (n,γ) experiments,[8] but is not observed in our Coulomb excitation measurements.

(c) The upper one is found at 1.039 MeV. Its associated band is observed in our experiment up to $I = \frac{23}{2}^-$

However, we obtain in both calculations only two quite strongly mixed $\frac{3}{2}^-$ bands. The first one, mainly $\frac{3}{2}^-\{[501]+[701]\}$, appears at 0.94 MeV (^{234}U core calculation) and 1.35 MeV (^{236}U core calculation). The upper one, mainly $\frac{3}{2}^-\{[761]+[741]\}$, appears, respectively, in both calculations at 1.20 and 1.78 meV. Mixing ratios in these two calculated bands can be found in Tables VI and VII.

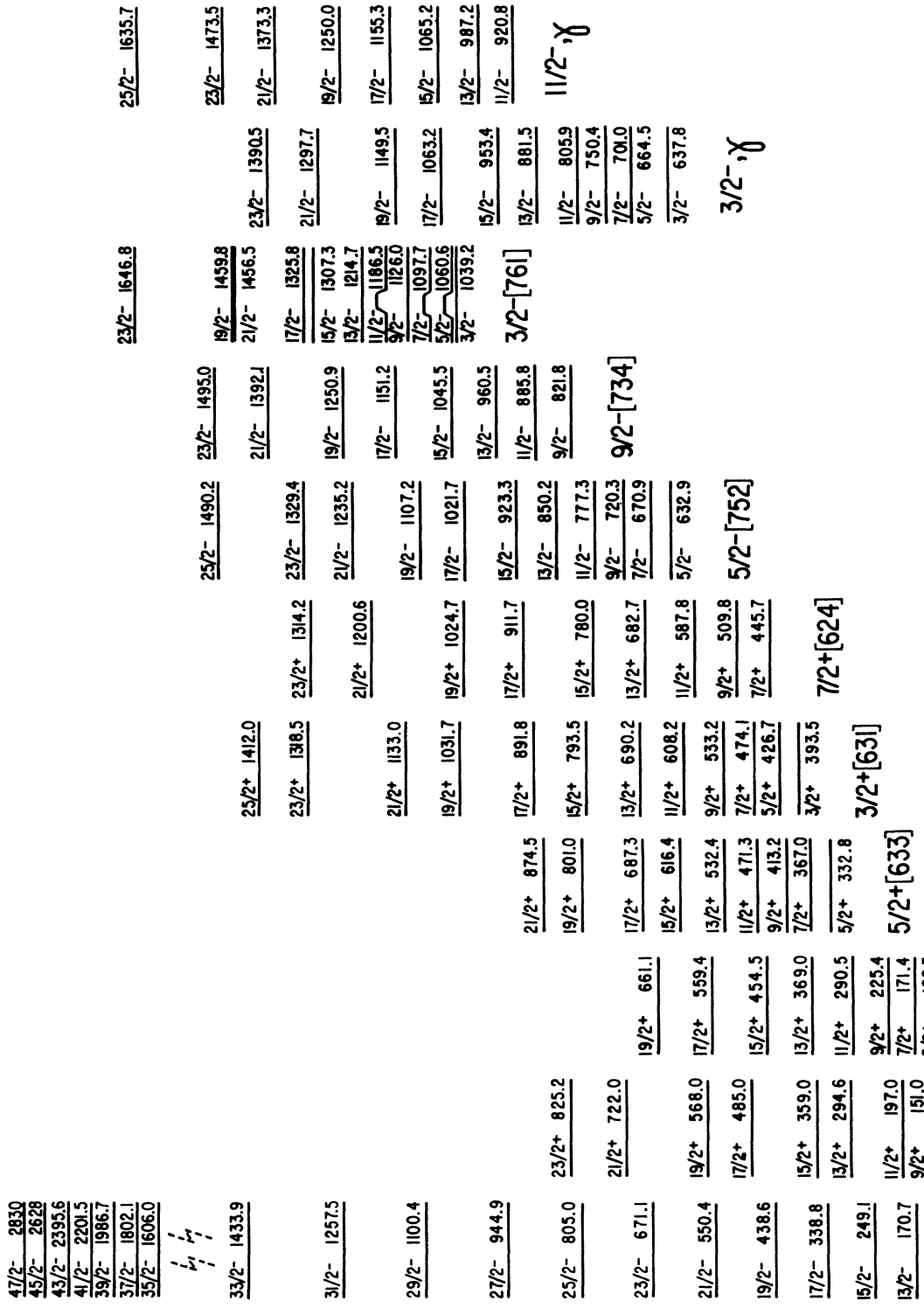

FIG. 16. Summary of the levels observed in ^{235}U by multiple Coulomb excitation with ^{84}Kr.

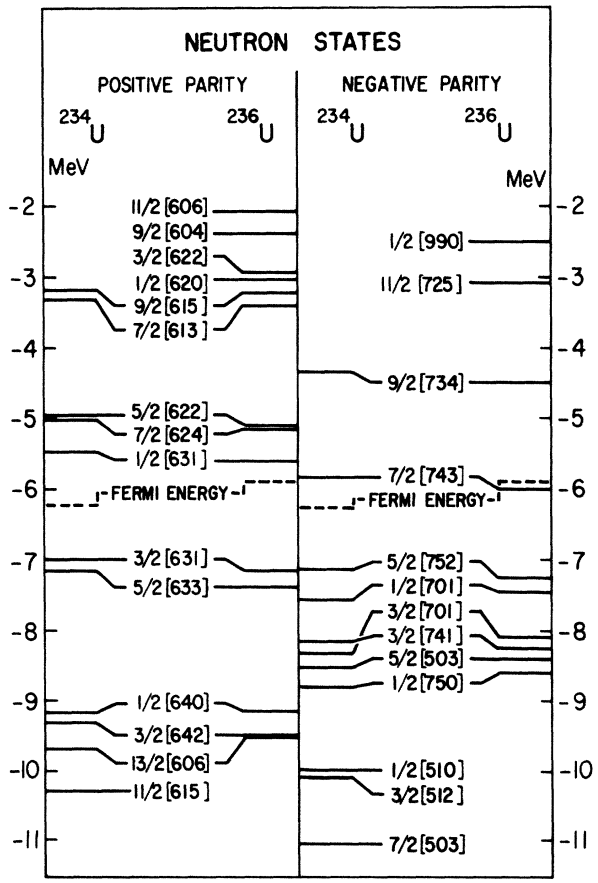

FIG. 17. Neutron single states around the Fermi level for the HF plus BCS equilibrium state of ^{234}U and ^{236}U. Each state is labeled by its major component on the deformed oscillator basis $K^{\pi}[N,N_z,\Lambda]$ with the usual notations.

Let us discuss the assignment of the lowest experimental $\frac{3}{2}^-$ band at 0.638 MeV.

(i) A $\frac{3}{2}^-\{[761]+[741]\}$ assignment for this band is very improbable because it is calculated at an energy which is far beyond the generally observed agreement of our calculations with experiment.

(ii) A $\frac{3}{2}^-\{[501]+[701]\}$ assignment is also excluded due to the values of $B(E2)$ transition probabilities to the ground-state band. As discussed in Ref. 23, such an assignment would lead to a factor of 100—1000 for the experimental versus calculated values.

(iii) Finally, this band does not correspond to any calculated state. This is consistent with the previous assignment[4] as a vibrational $\frac{3}{2}^-\{\frac{7}{2}^-[743], 2^+_\gamma\}$ structure. In addition, the strong Coulomb excitation of this band also favors this vibrational interpretation.

The second $\frac{3}{2}^-$ band head, found experimentally at 0.806 MeV, has already been proposed[8] as a Coriolis mixing of states built on $\frac{3}{2}^-[501]$ and $\frac{3}{2}^-[761]$. Our corresponding calculated band head $\frac{3}{2}^-$, mainly $\{[501]+[701]\}$, lies close enough to this level to confirm such an assignment.

This third experimental band starting at 1.039 MeV is strongly perturbed. It would thus be well reproduced by our calculated $\frac{3}{2}^-$, mainly $\{[761]+[741]\}$. The latter is indeed perturbed in our calculations, whereas the $\frac{3}{2}^-$, mainly $\{[501]+[701]\}$, band is not. This supports their respective assignments even though the energy agreement is rather poor especially in the ^{236}U core calculation. Furthermore, as pointed out in Sec. III A 4, the 1039 keV band is strongly populated by Coulomb excitation, which would support the $\frac{3}{2}^-\{[761]+[741]\}$ assignment, since the $\frac{3}{2}^-[761]$ state and the $\frac{7}{2}^-[743]$ ground state stem from the same $j\frac{15}{2}$ subshell.

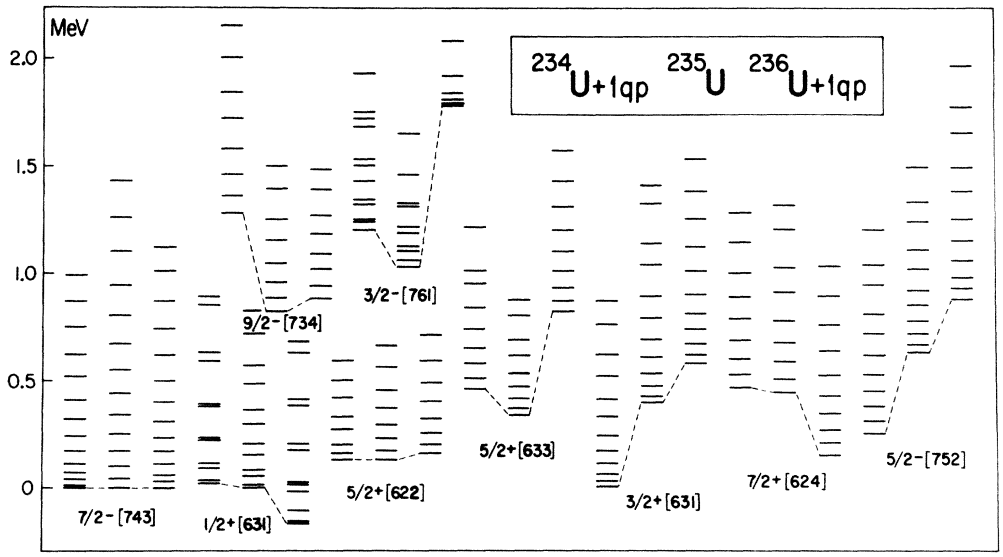

FIG. 18. Comparison between calculated and measured rotational bands in ^{235}U. Theoretical level sequences, given by ^{234}U and ^{236}U core calculations, are reported, for each band, on the left or right hand side of our corresponding experimental data. Rotational bands not observed in our Coulomb excitation measurement have been excluded from this comparison.

TABLE IV. Electric and relative magnetic reduced transition probabilities from or to levels of the $\frac{5}{2}^-[752]$ band. Experimental data are extracted from Refs. 4 and 7. Calculated value on the upper (lower) line of each part of the table corresponds to ^{234}U (^{236}U) core calculations. $E2$ reduced transition probabilities are expressed in $e^2\,\mathrm{fm}^4$.

Reduced transition probability		Experimental	Calculated
$B(E2)$	$\frac{7}{2}^-$ g.s. to $\frac{5}{2}\{\frac{5}{2}^-[752]\}$	$(2.1\pm0.3)\times10^2$	3.2×10^3
			5.5×10^2
$B(E2)$	$\frac{7}{2}^-$ g.s. to $\frac{7}{2}\{\frac{5}{2}^-[752]\}$	$\sim2.3\times10^2$	2.9×10^3
			5.4×10^2
$B(E2)$	$\frac{7}{2}^-$ g.s. to $\frac{9}{2}\{\frac{5}{2}^-[752]\}$	$(1.3\pm0.4)\times10^2$	5.6×10^3
			3.5×10^2
$B(E2)$	$\frac{7}{2}^-$ g.s. to $\frac{11}{2}\{\frac{5}{2}^-[752]\}$	$\sim0.46\times10^2$	2.1
			1.2×10^2
$B(M1)$	$\frac{7}{2}\{\frac{5}{2}^-[752]\}$ to $\frac{7}{2}^-$ g.s.	0.27 ± 0.04	0.20
relative			0.27
	$\frac{7}{2}\{\frac{5}{2}^-[752]\}$ to $\frac{9}{2}^-$ g.s.	1.0	1.0
			1.0
$B(M1)$	$\frac{9}{2}\{\frac{5}{2}^-[752]\}$ to $\frac{7}{2}^-$ g.s.	<0.1	0.11
relative			10^{-3}
	$\frac{9}{2}\{\frac{5}{2}^-[752]\}$ to $\frac{9}{2}^-$ g.s.	0.32 ± 0.11	0.23
			0.64
	$\frac{9}{2}\{\frac{5}{2}^-[752]\}$ to $\frac{11}{2}^-$ g.s.	1.0	1.0
			1.0
$B(M1)$	$\frac{11}{2}\{\frac{5}{2}^-[752]\}$ to $\frac{9}{2}^-$ g.s.	<0.2	0.21
relative			0.015
	$\frac{11}{2}\{\frac{5}{2}^-[752]\}$ to $\frac{11}{2}^-$ g.s.	~0.3	0.22
			1.25
	$\frac{11}{2}\{\frac{5}{2}^-[752]\}$ to $\frac{13}{2}^-$ g.s.	1.0	1.0
			1.0

5. *Vibrational $\frac{11}{2}^-$ and other negative parity bands*

A $\frac{11}{2}^-$ band is observed at 0.921 MeV. Such an $\frac{11}{2}^-$ rotational structure does not appear in our calculations below 2.3 MeV. This absence is indeed in agreement with the vibrational assignment $\frac{11}{2}^-\{\frac{7}{2}^-[743], 2_\gamma^+\}$ previously given.[4] This vibrational character is moreover related to some experimental remarks given in Sec. III.

In the same way, the vibrational band $\frac{1}{2}^-\{\frac{1}{2}^+[631], 0^-\}$ at 0.761 MeV,[7,8] not observed in our experiment, does not correspond to any possible rotational assignment in the present calculations.

A $\frac{1}{2}^-\{[701]+[501]\}$ band head is calculated at 0.25 and 0.66 MeV in both calculations. This kind of band is not favored in our Coulomb excitation experiment. However, such a band has been found in other experiments[7,8] with a $\frac{1}{2}^-$ band head at 650 keV identified as a $\frac{1}{2}^-[501]$ state. We thus confirm this assignment and note its strongly perturbed energy sequence in full agreement with the measured data. Furthermore, this perturbation is only due to internal Coriolis coupling (decoupling factor phenomena), thus excluding almost any band mixing.

Only one calculated band under 2 MeV does not correspond up to now to a measured band. This concerns a $\frac{5}{2}^-$ band built on the $\frac{5}{2}^-[503]$ intrinsic state and not mixed in both calculations up to $I=\frac{15}{2}$. The band head is given in the ^{234}U (^{236}U) core description at 1.160 MeV (1.590 MeV).

Some authors have suggested that the $\frac{1}{2}^-[770]$ single particle state should play some role in the level scheme. It

TABLE V. Same as Table IV for transitions from or to levels of the $\frac{9}{2}^-[734]$ band.

Reduced transition probability		Experimental	Calculated
$B(E2)$	$\frac{7}{2}^-$ g.s. to $\frac{9}{2}\{\frac{9}{2}^-[734]\}$	$(1.9\pm0.3)\times10^2$	4.2×10^3
			5.9×10^3
$B(E2)$	$\frac{7}{2}^-$ g.s. to $\frac{11}{2}\{\frac{9}{2}^-[734]\}$	$(1.7\pm0.4)\times10^2$	2.0×10^2
			2.7×10^2
$B(M1)$	$\frac{9}{2}\{\frac{9}{2}^-[734]\}$ to $\frac{7}{2}^-$ g.s.	1.0	1.0
relative			1.0
	$\frac{9}{2}\{\frac{9}{2}^-[734]\}$ to $\frac{9}{2}^-$ g.s.	0.48 ± 0.09	0.23
			0.10
	$\frac{9}{2}\{\frac{9}{2}^-[734]\}$ to $\frac{11}{2}^-$ g.s.	~0.3	0.018
			0.13
$B(M1)$	$\frac{11}{2}\{\frac{9}{2}^-[734]\}$ to $\frac{9}{2}^-$ g.s.	1.0	1.0
relative			1.0
	$\frac{11}{2}\{\frac{9}{2}^-[734]\}$ to $\frac{11}{2}^-$ g.s.	0.62 ± 0.13	0.35
			0.07
	$\frac{11}{2}\{\frac{9}{2}^-[734]\}$ to $\frac{13}{2}^-$ g.s	<0.2	0.07
			0.39
$B(M1)$	$\frac{13}{2}\{\frac{9}{2}^-[734]\}$ to $\frac{11}{2}^-$ g.s.	1.0	1.0
relative			1.0
	$\frac{13}{2}\{\frac{9}{2}^-[734]\}$ to $\frac{13}{2}^-$ g.s.	0.8 ± 0.3	0.82
			0.5

is worth noting that the corresponding band head does not appear in our calculations under 2.5 MeV.

6. *The $\frac{1}{2}^+[631]$ band at 0.1 keV*

We confirm the identification of this band, which indeed appears in our calculations at a very low energy. The two different core descriptions yield a very much perturbed energy sequence, as found experimentally. The ^{236}U core calculation describes it as a quasipure band, whereas in the ^{234}U core calculation, it is found to be weakly mixed with the $\frac{3}{2}^+[631]$ and sometimes (at spins $\frac{9}{2}^+$ and $\frac{15}{2}^+$) strongly mixed with the lower $\frac{5}{2}^+$ band. Its mixing with the $\frac{3}{2}^+[631]$ could be related to the observed strong decay from this last band to the $\frac{1}{2}^+[631]$ band.

7. *The $\frac{3}{2}^+[631]$ band at 0.394 MeV*

The assignment of this band is confirmed by our calculations, which predict it to be in a large but compatible range of energy between 0.004 MeV (^{234}U-core calculation) and 0.580 MeV (^{236}U-core calculation). This band is also found to be a quasipure rotational band in the ^{236}U core calculation. In the ^{236}U-core calculation it is weakly coupled with the $\frac{1}{2}^+[631]$ and with the lowest $\frac{5}{2}^+$ band. The latter calculation may explain the observed preferential connections of this band, as discussed in Secs. III B 2.

8. *The two $\frac{5}{2}^+$ bands at 0.129 and 0.333 MeV*

Our rotor-plus-quasiparticle calculation based on the ^{234}U core predicts a lower $\frac{5}{2}^+$ state at 0.13 MeV with the $\frac{5}{2}^+[633]$ label and a higher one, $\frac{5}{2}^+[622]$, at 0.46 MeV. On the opposite side, ^{236}U core calculations give the assignments $\frac{5}{2}^+[622]$ for the lower one at 0.16 MeV and $\frac{5}{2}^+[633]$ for the other at 0.82 MeV.

At first sight the experimental results and previous assignments seem to be in better agreement with the ^{236}U-core calculation. However, it could be noticed that this latter calculation gives a rather poor agreement for the higher $\frac{5}{2}^+$ band-head energy. On the other hand, the ^{234}U-core calculation also appears to be in reasonable agreement with experiment. It is appropriate to analyze in a more detailed way the mixing ratios in these calculated $\frac{5}{2}^+$ bands (see Tables VIII and IX). As already observed in most of the bands, the ^{234}U-core calculation yields generally more mixed states. A [622] label has been proposed for the lower $\frac{5}{2}^+$ band due to its connections to the $\frac{1}{2}^+[631]$ and $\frac{3}{2}^+[631]$ bands. However, we do find in our calculated $\frac{5}{2}^+[633]$ band (^{234}U-core calculation) that there is a significant $\frac{1}{2}^+[631]$ and $\frac{3}{2}^+[631]$ admixture, which also goes along with the same experimental feature. The two calculated bands for this ^{234}U-core calculation exhibit, anyway, a common mixing with the $\frac{7}{2}^+[624]$ structure which could explain their favored interconnections.

TABLE VI. Same as Table II for Coriolis mixing in the $\frac{3}{2}^-[501]$ band. For each level the upper (lower) line corresponds to the ^{234}U core (^{236}U core) calculation. This calculated band is to be compared to the experimental band head proposed (Ref. 8) at 0.806 MeV, which was not observed in our Coulomb excitation measurements.

State I	Energy (MeV)	$\frac{3}{2}^-\{[501]+[701]\}$	$\frac{3}{2}^-\{[761]+[741]\}$	$\frac{1}{2}^-[750]$	$\frac{5}{2}^-[503]$	$\frac{5}{2}^-[752]$
$\frac{3}{2}$	0.94	73	27			
	1.35	80	20			
$\frac{5}{2}$	0.98	73	27			
	1.39	79	20			
$\frac{7}{2}$	1.02	71	28			
	1.44	79	19			
$\frac{9}{2}$	1.09	72	26			
	1.51	77	21			
$\frac{11}{2}$	1.16	65	30			
	1.58	77	18			
$\frac{13}{2}$	1.24	71	25			
	1.68	74	21			
$\frac{15}{2}$	1.33	49	37	7		
	1.77	74	14	5	4	
$\frac{17}{2}$	1.45	71	23		5	
	1.90	71	22		5	
$\frac{19}{2}$	1.61	70		19	4	5
	2.00	64	8	14	4	9
$\frac{21}{2}$	1.70	70	22		6	
	2.17	69	23		6	
$\frac{23}{2}$	1.86	81		7	7	
	2.27	43		28	4	19

One has therefore to bear in mind some possible ambiguity on the assignment $\frac{5}{2}^+[622]$ and $\frac{5}{2}^+[633]$ of these two bands. As a result, the present analysis is not able to confirm or invalidate the previous assignments of these bands, which are presented in Fig. 18 under their usual labels (calculated $\frac{5}{2}^+$ bands are shown in order of appearance, whatever their main components). Some further calculations of reduced transition probabilities might answer this question.

9. *The $\frac{7}{2}^+[624]$ band at 0.446 MeV*

Our calculations reproduce reasonably well such a band (especially the ^{234}U-core calculations). We therefore confirm the previous $\frac{7}{2}^+[624]$ assignment proposed in Ref. 4. Calculated bands exhibit Coriolis mixing with the $\frac{5}{2}^+[622]$ assignment (and also with the $\frac{5}{2}^+[633]$ one, only in the ^{234}U-core calculation). These mixing ratios are coherent with the observed preferential decay of this band to both $\frac{5}{2}^+$ bands. The ^{234}U-core description seems therefore somewhat better. Of course, a possible vibrational component of this $\frac{7}{2}^+$ band, suggested in Ref. 8, cannot be excluded, until new information about experimental transition probabilities is available.

10. *Other positive parity bands*

Different other vibrational structures have been observed in other experiments and identifications have been

TABLE VII. Same as Table II for Coriolis mixing in the $\frac{3}{2}^-\{[761]+[741]\}$ band. For each level, the upper (lower) line corresponds to the ^{234}U core (^{236}U core) calculation. The experimental corresponding band is proposed to be the $\frac{3}{2}^-$ band starting at 1.038 MeV and strongly excited in our Coulomb excitation measurements.

State I	Energy (MeV)	$\frac{3}{2}^-\{[761]+[741]\}$	$\frac{3}{2}^-\{[501]+[701]\}$	$\frac{1}{2}^-[750]$	$\frac{5}{2}^-[752]$	$\frac{9}{2}^-[734]$
$\frac{3}{2}$	1.20	71	26			
	1.78	75	19	6		
$\frac{5}{2}$	1.24	70	26			
	1.81	75	18	5		
$\frac{7}{2}$	1.25	57	27	13		
	1.79	59	11	27		
$\frac{9}{2}$	1.34	63	26	6	4	
	1.92	69	16	10	5	
$\frac{11}{2}$	1.32	39	25	25	5	
	1.84	46	4	43	7	
$\frac{13}{2}$	1.50	53	23	8	8	
	2.08	63	14	13	10	
$\frac{15}{2}$	1.43	19	39	31	8	
	2.40	36	16	44	4	
$\frac{17}{2}$	1.68	24	14	5	4	48
	1.72	26	11	5	8	44
	2.31	57	12	15	15	
$\frac{19}{2}$	1.53	44	17	26	10	
	2.95	39	17	38	6	
$\frac{21}{2}$	1.93	30	19	8	8	29
	2.59	51	11	17	20	
$\frac{23}{2}$	2.67	43	7	45	5	
	3.30	40	18	33	8	

proposed[7,8] as follows: $\frac{1}{2}^+\{\frac{1}{2}^+[631], 0_\beta^+\}$ at 0.769 MeV, $\frac{1}{2}^+\{\frac{5}{2}^+[622], 2_\gamma^+\}$ at 0.843 MeV, $\frac{5}{2}^+\{\frac{5}{2}^+[622], 0_\beta^+\}$ at 0.905 MeV, and $\frac{1}{2}^+\{\frac{3}{2}^+[631], 2_\gamma^+\}$ at 0.968 MeV.

It is gratifying that none of these bands receives any possible assignment in our calculations, which indirectly confirms their nonrotational character, since all calculated positive parity bands whose band heads are located below 2 MeV have been matched with an experimental band.

C. Moments of Inertia

In order to visualize in a clearer way the relative energies within each rotational band, it is convenient to extract the moment of inertia corresponding to a given $I+2\rightarrow I$ transition. The variation of this quantity with respect to I may be understood as a measure of the Coriolis coupling of the considered band. Such results are displayed in Fig. 19 (the moments of inertia are normalized to the $I_0+1\rightarrow I_0$ transition, where I_0 is the bandhead spin).

It is clearly seen that our calculations somewhat overestimate the Coriolis coupling for the ground state band, as already mentioned. The agreement is significantly better for the other bands, such as, for instance, the $\frac{9}{2}^-[734]$, $\frac{1}{2}^+[631]$, and $\frac{3}{2}^+[631]$ with the ^{234}U core, or the $\frac{5}{2}^-[752]$ with the ^{236}U core.

TABLE VIII. Same as Table II for Coriolis mixing in the lower calculated $\frac{5}{2}^+$ band. For each level the upper (lower) line corresponds to the ^{234}U core (^{236}U core) calculation.

State I	Energy (MeV)	$\frac{5}{2}^+[622]$	$\frac{5}{2}^+[633]$	$\frac{1}{2}^+[631]$	$\frac{7}{2}^+[624]$	$\frac{3}{2}^+[631]$
$\frac{5}{2}$	0.13		>95			
	0.16	>95				
$\frac{7}{2}$	0.16		>95			
	0.20	>95				
$\frac{9}{2}$	0.20		48	47		
	0.25	90			7	
$\frac{11}{2}$	0.27		84	4	8	
	0.32	85			10	4
$\frac{13}{2}$	0.33		83	6	10	
	0.40	80			14	4
$\frac{15}{2}$	0.42		51	31	8	9
	0.49	75			17	5
$\frac{17}{2}$	0.50		79	4	13	
	0.59	71			19	5
$\frac{19}{2}$	0.59		57	30	11	
	0.71	67			22	7
$\frac{21}{2}$	0.71		75	4	16	
	0.83	65			22	7

TABLE IX. Same as Table II for Coriolis mixing in the upper calculated $\frac{5}{2}^+$ band. For each level the upper (lower) line corresponds to the ^{234}U core (^{236}U core) calculation.

State I	Energy (MeV)	$\frac{5}{2}^+[622]$	$\frac{5}{2}^+[633]$	$\frac{7}{2}^+[624]$	$\frac{3}{2}^+[631]$
$\frac{5}{2}$	0.46	>95			
	0.82		>95		
$\frac{7}{2}$	0.51	93		5	
	0.87		>95		
$\frac{9}{2}$	0.58	86		9	
	0.93		>95		
$\frac{11}{2}$	0.65	80		14	4
	1.01		>95		
$\frac{13}{2}$	0.74	74	>95	17	5
	1.10				
$\frac{15}{2}$	0.84	69		20	6
	1.20		94		

TABLE IX. (*Continued*).

State I	Energy (MeV)	$\frac{5}{2}^+[622]$	$\frac{5}{2}^+[633]$	$\frac{7}{2}^+[624]$	$\frac{3}{2}^+[631]$
$\frac{17}{2}$	0.95	64		22	7
	1.31		92	4	
$\frac{19}{2}$	1.08	61		24	7
	1.43		91	5	
$\frac{21}{2}$	1.21	58		26	8
	1.56		89	5	

V. CONCLUSIONS

For such a stiffly deformed nucleus, a unified model description in the rotor-plus-quasiparticle approach seemed *a priori* well suited. In view of the recent theoretical progress concerning the microscopic evaluation of the potential and kinetic energy part of the Bohr Hamiltonian, it was timely to collect the most complete set of data to provide the theory with a broad testing ground.

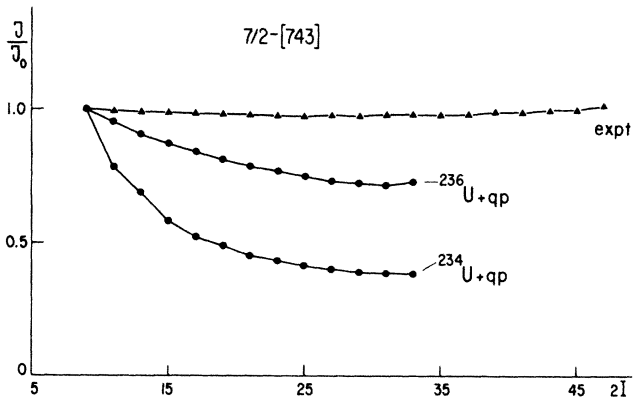

FIG. 19. The normalized moment of inertia J/J_0 in the $\frac{7}{2}^-[743]$ ground state band as function of the spin. The moment of inertia of the experimental and the two calculated bands has been determined under the pure rotor assumption without coupling, $E(I)=(\hbar^2/2J)[I(I+1)-I_0(I_0+1)]$. The normalization of the moment of inertia J_0 has been deduced from the $\frac{9}{2}\rightarrow\frac{7}{2}$ transition.

The experimental results extracted from the present work represent the most complete set of rotational sequences established for odd-A uranium nuclei. With the degree of development reached, the behavior of each band is well reproduced.

Without any adjustable parameter the rotor-plus-quasiparticle approach has been able to confirm or identify eleven rotational bands resulting from the coupling of quasiparticle and rotor degrees of freedom and to assess the vibrational character for seven others. The quality of the reproduction of band-head energies, moments of inertia, multiple moments, and transition probabilities allows us to conclude the relevance of the HF plus BCS wave functions. Even though the whole approach is somewhat crude in its collective dynamical assumptions, it appears to provide a useful tool since it allows one to distinguish the main band structures in such rather complicated schemes. It provides also comparative grounds for further theoretical developments as the explicit inclusion of the gamma degree of freedom and a coupling of the quasiparticle and quadrupole collective degrees of freedom, relaxing, then, the limitative assumption of a delta peaked collective wave function.

[1]Ch. Briançon and I. N. Mikhailov, Fiz. Elem. Chastits At. Yadra **13**, 245 (1985) [Sov. J. Part. Nucl. **13**, 101 (1982)].

[2]D. Schwalm, in Proceedings of the International Conference on High Angular Momentum Properties of Nuclei, Oak Ridge (Nov. 1982) (unpublished).

[3]A. Lefebvre, thèse d'Etat, Université Orsay, 1984.

[4]F. S. Stephens, M. P. Holtz, R. M. Diamond, and J. O. Newton, Nucl. Phys. **A115**, 129 (1968).

[5]R. S. Simon, F. Folkmann, Ch. Briançon, J. Libert, J. P. Thibaud, R. J. Walen, and S. Frauendorf, Z. Phys. A **298**, 121 (1980).

[6]R. Kulessa, R. P. deVito, H. Emling, E. Grosse, D. Schwalm, R. S. Simon, A. Lefebvre, Ch. Briancon, R. J. Walen, G. Sletten, and Z. Phys. A **312**, 135 (1983).

[7]M. R. Schmorak, Nucl. Data. Sheets **40**, 35 (1983).

[8]J. Almeida, T. von Egidy, R. H. M. van Assche, M. G. Borner, W. F. Davidson, K. Schreckenbach, and A. I. Namenson, Nucl. Phys. **A315**, 71 (1979).

[9]J. de Bettencourt, Ch. Briançon, J. Libert, J. P. Thibaud, R. J. Walen, A. Gizon, and Ph. Quentin, Centre de Spectrométrie Nucléaire et de Spectrométrie de Masse Annual Report (1976—77), p. 28 (unpublished); J. de Bettencourt, Ch. Briançon, A. Gizon, J. C. Jacmart, J. Libert, J. P. Thibaud, and R. J. Walen, Proceedings of the International Conference on Nuclear Structure, Tokyo, Sept. 1977, p. 461 (unpublished).

[10]J. de Bettencourt, Ch. Briançon, J. Libert, J. P. Thibaud, R. J. Walen, Ph. Quentin, and A. Gizon, in Proceedings of the Symposium on High Spin Phenomena in Nuclei, Argonne, March 1979, p. 487 (unpublished); J. de Bettencourt, Ch. Briancon, J. Libert, J. P. Thibaud, R. J. Walen, A. Gizon, M. Meyer, Ph. Quentin, CSNSM Annual Report, 1978–80, p. 39 (unpublished).

[11]F. Rickey, E. Jurney, and H. Britt, Phys. Rev. C **5**, 2072 (1972).

[12]F. Sterba, J. Sterbova, and J. Kvasil, Czech. J. Phys. B **28**, 31 (1978).

[13]R. C. Thompson, J. R. Huizenga, and Th. W. Elze, Phys. Rev. C **13**, 638 (1976).

[14]T. H. Braid, R. Chasman, J. R. Erskine, and M. M. Friedman, Phys. Rev. C **1**, 275 (1970).

[15]J. E. Cline, Nucl. Phys. **A106**, 481 (1968).

[16]F. Horch, Z. Phys. **194**, 405 (1966).

[17]T. Elze and J. R. Huizenga, Nucl. Phys. **A133**, 10 (1969).

[18]M. Meyer, J. Danière, J. Letessier, and Ph. Quentin, Nucl. Phys. **A316**, 93 (1979).

[19]M. G. Desthuilliers-Porquet, M. Meyer, and Ph. Quentin, in Proceedings of the 4th International Conference on Nuclei far from stability, Helsingør (1981) (unpublished); Centre Européen de Recherches Nucléaires, Report No. 8108, p. 623 (unpublished).

[20]J. Sauvage, M. G. Porquet, M. Meyer, and Ph. Quentin, Nucl. Phys. **A451**, 365 (1986).

[21]M. Meyer, Ann. Phys. (Paris) **9**, 791 (1984).

[22]Ph. Quentin, M. Meyer, J. Letessier, J. Libert, and M. G. Desthuilliers-Porquet, in *Nuclear Spectroscopy of Fission Products,* edited by T. V. Egidy (Institute of Physics, Bristol, 1980), p. 280.

[23]J. Libert, M. Meyer, and Ph. Quentin, Phys. Rev. C **25**, 586 (1982).

[24]M. Beiner, H. Flocard, Nguyen Van Giai, and Ph. Quentin, Nucl. Phys. **A238**, 29 (1975).

[25]D. Vautherin, Phys. Rev. C **7**, 296 (1973).

[26]H. Flocard, Ph. Quentin, A. K. Kerman, and D. Vautherin, Nucl. Phys. **A203**, 433 (1973).

[27]Ph. Quentin and H. Flocard, Annu. Rev. Nucl. Part. Sci. **28**, 523 (1978).

[28]D. Vautherin and D. M. Brink, Phys. Rev. C **5**, 626 (1972).

[29]M. Cailliau, J. Letessier, H. Flocard, and Ph. Quentin, Phys. Lett. **46B**, 11 (1973).

[30]J. Sauvage-Letessier, Ph. Quentin, and H. Flocard, Nucl. Phys. **A370**, 231 (1981).

[31]X. Campi and M. Epherre, Phys. Rev. C **22**, 2605 (1980).

[32]J. Libert, M. Meyer, and Ph. Quentin, unpublished calculation for erbium isotopes.

[33]H. Flocard, Ph. Quentin, and D. Vautherin, Phys. Lett. **46A**, 104 (1973).

[34]H. Flocard and Ph. Quentin, unpublished calculations for *s-d* shell nuclei.

[35]P. Quentin, in *Nuclear Self Consistent Fields,* edited by G. Ripka and M. Porneuf (North-Holland, Amsterdam, 1975), p. 297.

[36]J. Libert and Ph. Quentin, Phys. Rev. C **25**, 571 (1982).

[37]C. E. Bemis, Jr., F. K. McGowan, J. L. C. Ford, Jr., W. T. Milner, P. H. Stelson, and R. L. Robinson, Phys. Rev. C **8**, 1466 (1973).

[38]*Table of Isotopes,* 7th ed., edited by C. M. Lederer and V. S. Shirley (Wiley, New York, 1978).

[39]J. D. Zumbro, E. B. Shera, Y. Tanaka, C. E. Bemis, Jr., R. A. Naumann, M. V. Hoehn, W. Reuter, and R. M. Steffen, Phys. Rev. Lett. **53**, 1888 (1984).

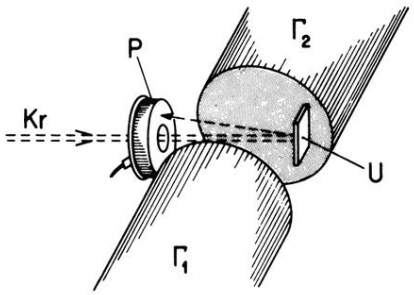

FIG. 1. Experimental setup to study Coulomb excitation of ^{235}U with ^{84}Kr projectiles. The annular particle detector was protected against x rays and electrons by a thin gold foil. It detected scattered krypton projectiles in an angle of 133°—147° with respect to the beam axis. The two γ counters, γ_1 and γ_2, were located at 90° on either side of the incident beam.